ME338A - Final project - Paper review - due in class Thu, March 12, 2009, 11am

Constitutive modelling of passive myocardium

A structurally-based framework for material characterization

Gerhard A. Holzapfel & Ray W. Ogden

Philosophical Transactions of the Royal Society A, accepted for publication, 2009.

This final project will demonstrate that during the past 10 weeks, you have learned to read state of the art continuum mechanics literature. Gerhard Holzapfel and Ray Ogden have submitted this manuscript for publication and agreed that you could read and review it before it is actually published. It introduces a new continuum mechanics model for passive cardiac muscle tissue similar to the one we have dissected in class.

1 Read the publication and try to understand what it is all about. You do not necessarily need to understand **all** the equations. You can briefly glance over section 6, it is not relevant for this final project.

2 Summarize the manuscript in less than 200 words.

3 Ogden & Holzapfel use a slightly different notation than we have used in class, i.e., they do not use dots to indicate scalar products. Rewrite equations (3.1) to (3.14) in our tensor notation, i.e., use the dot for scalar products when appropriate.

4 Rewrite equations (3.1) to (3.14) in index notation. For each equation, state in brackets whether it is a scalar, vectorial, or second order tensorial equation.

5 In section 4, Ogden & Holzapfel review existing constitutive models for passive cardiac tissue. They discuss three transversely isotropic models (4.1), (4.2), and (4.3) and three orthotropic models (4.5), (4.7), and (4.8). Summarize these six models in a table. For each model, list the first author, the year it was published, the invariants it is based on, and the parameters that are needed.

6 In figure 4, image (a) represents the deformation state you had to analyze in your midterm. Calculate the Green Lagrange strain tensor $\boldsymbol{E} = \frac{1}{2}\,[\,\boldsymbol{F}^{\mathrm{t}} \cdot \boldsymbol{F} - \boldsymbol{I}\,]$ from the deformation gradient given in (5.9) and sketch the deformed configuration in the fs-plane.

7 Equation (5.38) is the key equation of the paper. It introduces the free energy function for myocardial tissue. Describe its three terms and explain the required material parameters.

8 Most soft biological tissues are incompressible and anisotropic. How is incompressibility and anisotropy handled in the constitutive formulation?

9 Review the publication with the help of the attached spreadsheet. Use common sense to answer the questions you cannot answer based on your current continuum mechanics knowledge. There are no wrong answers, and we will not take off points as long as you can justify your opinion.

Instructions

Please rate this manuscript on a scale of 1-5, with 1 indicating greatest degree or best, and 5 indicating least degree or poor. You must also provide comments to the authors in prose. It is not acceptable to merely fill out numbers, and return the review.

Manuscript title ______________________________

Authors ______________________________

Summary (required brief summary of the context)

____
____
____
____
____
____

Presentation	(best) 1	2	3	4	5 (poor)
is clearly written	☐	☐	☐	☐	☐
title is appropriate	☐	☐	☐	☐	☐
abstract is appropriate	☐	☐	☐	☐	☐
figures and tables are adequate	☐	☐	☐	☐	☐
problem statement is clear	☐	☐	☐	☐	☐
provides appropriate detail	☐	☐	☐	☐	☐
describes limitations	☐	☐	☐	☐	☐
references are adequate	☐	☐	☐	☐	☐

Comments (required in addition to the number ratings above)

____
____
____

Significance	(best) 1	2	3	4	5 (poor)
represents important advance	☐	☐	☐	☐	☐
addresses importand and realistic problem	☐	☐	☐	☐	☐
is likely to scale up to realistic problems	☐	☐	☐	☐	☐
provides new evidence for existing technique	☐	☐	☐	☐	☐

Comments (required in addition to the number ratings above)

___

___

___

Originality	(best) 1	2	3	4	5 (poor)
novel approach or combination of approaches	☐	☐	☐	☐	☐
has not been published before	☐	☐	☐	☐	☐
points out differences from related research	☐	☐	☐	☐	☐
reformulates a problem in an important way	☐	☐	☐	☐	☐

Comments (required in addition to the number ratings above)

___

___

___

Technical content	(best) 1	2	3	4	5 (poor)
evaluates effectiveness of techniques	☐	☐	☐	☐	☐
is supported with sound arguments	☐	☐	☐	☐	☐
is supported with theoretical analysis	☐	☐	☐	☐	☐
is supported with experimental results	☐	☐	☐	☐	☐
is technically sound	☐	☐	☐	☐	☐

Additional comments to the autors

___

___

___

Overall recommendation ☐ accept ☐ marginal ☐ reject

Your confidence in recommendation ☐ strong ☐ medium ☐ weak

Confidential commments to the editor

___

___

___

Confidential reviewer name ___

Constitutive modelling of passive myocardium. A structurally-based framework for material characterization

BY GERHARD A. HOLZAPFEL[1,2] † AND RAY W. OGDEN[3]

[1]*Royal Institute of Technology (KTH), Department of Solid Mechanics School of Engineering Sciences, Osquars Backe 1, 100 44 Stockholm, Sweden*

[2]*Institute for Biomechanics, Center for Biomedical Engineering Graz University of Technology, Kronesgasse 5-I, 8010 Graz, Austria*

[3] *Department of Mathematics, University of Glasgow University Gardens, Glasgow G12 8QW, UK*

Submitted to

***Philos. T. Roy. Soc. A*, February 1, 2009; Revised Version: March 2, 2009**

In this paper we first of all review the morphology and structure of the myocardium and discuss the main features of the mechanical response of passive myocardium tissue, which is an orthotropic material. Locally within the architecture of the myocardium three mutually orthogonal directions can be identified, forming planes with distinct material responses. We treat the left ventricular myocardium as a non-homogeneous, thick-walled, nonlinearly elastic and incompressible material and develop a general theoretical framework based on invariants associated with the three directions. Within this framework we review existing constitutive models and then develop a structurally based model that accounts for the muscle fibre direction and the myocyte sheet structure. The model is applied to simple shear and biaxial deformations and a specific form fitted to the existing (and somewhat limited) experimental data, emphasizing the orthotropy and the limitations of biaxial tests. The need for additional data is highlighted. A brief discussion of issues of convexity of the model and related matters concludes the paper.

Keywords: Myocardium; constitutive modelling; orthotropy; muscle fibres; myocyte sheet structure

1. Introduction

Of central importance for the better understanding of the fundamental mechanisms underlying ventricular mechanics are (i) realistic descriptions of the 3D geometry and structure of the myocardium, (ii) continuum balance laws and boundary conditions, and, most importantly, (iii) constitutive equations that characterize the material properties of the my-

† Author for correspondence (holzapfel@TUGraz.at).

ocardium, including their spatial and temporal variations, together with statistical parameter estimation and optimization and validation. In order to characterize the material properties it is essential to have available comprehensive force–deformation data from a range of different deformation modes. In particular, a combination of biaxial test data with different loading protocols and shear test data at different specimen orientations is required in order to capture adequately the direction-dependent nonlinear material response.

The purpose of the present paper is to develop a general theoretical framework within the context of nonlinear elasticity theory that takes account of the structural features of the myocardium and its orthotropic properties. Within that framework we then consider specific models for the myocardium in order to characterize its passive mechanical response. There are several models of the elasticity of the myocardium available in the literature, including isotropic models (see, for example, Demiray, 1976), transversely isotropic models (for example, Humphrey & Yin, 1987; Humphrey *et al.*, 1990; Guccione *et al.*, 1991; Costa *et al.*, 1996), and, more recently, orthotropic models (for example, Costa *et al.*, 2001; Hunter *et al.*, 1997; Schmid *et al.*, 2006). We review these and several others briefly in §4. For a recent account of modelling aspects of the mechanics of the heart and arteries we refer to the forthcoming edited volume by Holzapfel & Ogden (2009a).

One problem in developing an adequate constitutive model is the shortage of experimental data suitable for detailed parameter estimation in specific functional forms. Early contributions to gathering such data are contained in the work of Demer & Yin (1983) and Yin *et al.* (1987) in which data from biaxial tests were obtained. However, as we shall emphasize later, data from biaxial tests alone are not enough to characterize the passive response of myocardium since such data suggest that the material is transversely isotropic. That this is not the case has been demonstrated clearly in the more recent work by Dokos *et al.* (2002), which, on the basis of shear tests conducted on cube-shaped specimens from different orientations within the myocardium, highlighted the orthotropic behaviour of the material. It remains the case, however, that there is a need for more comprehensive sets of data to be obtained.

In §2 we outline the key features of the morphology and structure of the myocardium and then describe the passive mechanical response of myocardial tissue on the basis of the available biaxial and shear test data. Against this background we then construct, in §3, a general framework for the elastic strain-energy function based on the use of invariants that are related to the myocardium structure. This framework embraces most, if not all, of the elasticity-based constitutive models for the passive myocardium that have appeared in the literature to date. Next, in §4, as mentioned above, we review the existing models within this framework. In §5, guided by data from shear and biaxial tests, we develop an appropriately specialized form of the general strain-energy function from §3. This is then specialized further by the introduction of specific functional forms for the dependence of the energy function on the restricted set of invariants that it includes. The model so constructed is then evaluated against the considered shear and biaxial data and values of the material constants it contains are obtained by curve fitting. The general features of the shear data of Dokos *et al.* (2002) are reproduced by using six material constants, while eight constants are needed to recover finer details of the data. To fit the biaxial data a transversely isotropic specialization of the model suffices to give a reasonable fit to the data of Yin *et al.* (1987) and only four material constants are needed. This highlights the point already alluded to that biaxial tests alone are not sufficient to extract the orthotopic nature of the tissue and should not therefore be used in isolation.

In §6 we examine the form of strain-energy function constructed with reference to inequalities that ensure 'physically reasonable response', including the monotonicity of the stress deformation behaviour in uniaxial tests and notions of convexity and strong ellipticity in 3D. These all require, in particular, that the materials constants included in the various terms contributing to the strain-energy are positive, which is consistent with the values obtained in fitting the data. Finally, §7 is devoted to a concluding discussion.

2. Morphology, structure and typical mechanical behaviour of the passive myocardium

(*a*) *Morphology and structure*

The human heart consists of four chambers, namely the right and left *atria*, which receive blood from the body, and the left and right *ventricles*, which pump blood around the body. For a detailed description of the individual functionalities of these four chambers, see Katz (1977). There is still an ongoing debate concerning the structure of the heart (Gilbert *et al.*, 2007), and, in particular, the anisotropic cardiac microstructure. One approach describes the heart as a single muscle coiled in a helical pattern, while the other approach considers the heart to be a continuum composed of laminar sheets, an approach we are adopting in the present work.

The left ventricle has the largest volume of the four chambers and serves the particular purpose of distributing blood with a higher pressure than the right ventricle. As a consequence of the need to support higher pressure, the wall thickness of the left ventricle is larger than that of the right ventricle. The wall thickness and curvature of the left ventricle vary spatially; it is thickest at the base and at the equator and thinnest at its apex. The wall thickness and curvature also vary temporally through the cardiac cycle. The left ventricular wall may be regarded as a continuum of myocardial fibres, with a smooth transmural vari-

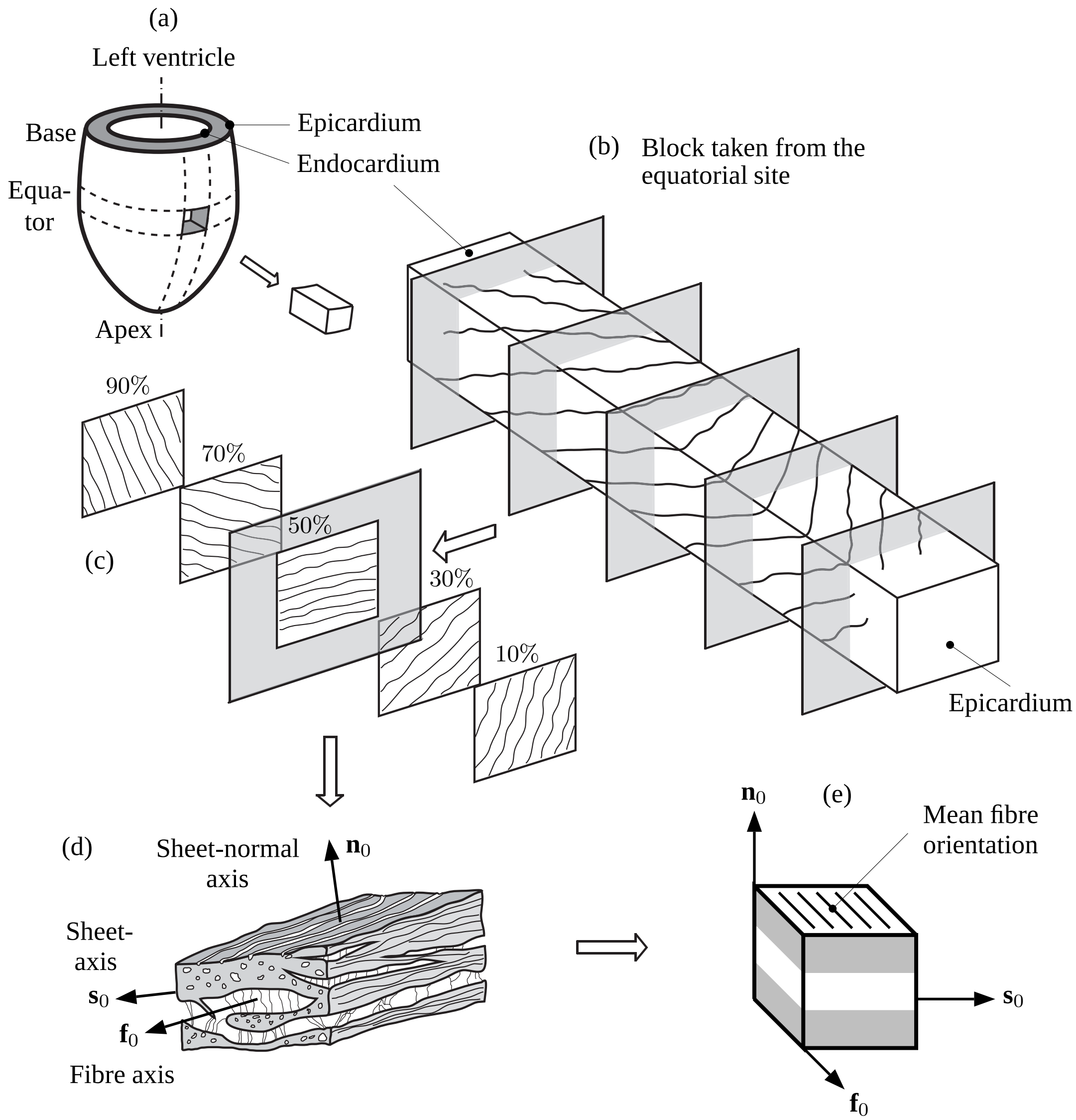

Figure 1. Schematic diagram of: (a) the left ventricle and a cut out from the equator; (b) the structure through the thickness from the epicardium to the endocardium; (c) five longitudinal–circumferential sections at regular intervals from 10–90% of the wall thickness from the epicardium showing the transmural variation of layer orientation; (d) the layered organization of myocytes and the collagen fibres between the sheets referred to a right-handed orthonormal coordinate system with fibre axis $\mathbf{f}_0$, sheet axis $\mathbf{s}_0$ and sheet-normal axis $\mathbf{n}_0$; (e) a cube of layered tissue with local material coordinates (X_1, X_2, X_3) serving the basis for the geometrical and constitutive model.

ation of the fibre orientations. It is modelled reasonably well as a thick-walled ellipsoid of revolution that is truncated at the base, as depicted in figure 1(a).

The heart wall consists of three distinct layers: an inner layer (the *endocardium*), a middle layer (the *myocardium*), and an outer layer (the *epicardium*). The endocardium lines the inside of the four chambers and it is a serous membrane, with approximate thickness $100\,\mu$m, consisting mainly of epimysial collagen, elastin and a layer of endothelial cells, the latter serving as an interfacial layer between the wall and the blood. The protective epicardium is also a membrane with thickness of the order of $100\,\mu$m and consists largely of epimysial collagen and some elastin.

In this paper we focus attention on the myocardium of the left ventricle. The ventricular myocardium is the functional tissue of the heart wall with a complex structure that is well represented in the quantitative studies of LeGrice *et al.* (1995, 1997), Young *et al.* (1998), and Sands *et al.* (2005). The left ventricular wall is a composite of layers (or sheets) of parallel myocytes which are the predominant fibre types, occupying about 70% of the volume. The remaining 30% consists of various interstitial components (Frank & Langer, 1974), while only 2–5% of the interstitial volume is occupied by collagen arranged in a spatial network that forms lateral connections between adjacent muscle fibres, with attachments near the z-line of the sarcomere. Figure 1(b) illustrates the change of the three-dimensional layered organization of myocytes through the wall thickness from the epicardium to the endocardium. In addition, figure 1(b) displays views of five longitudinal–circumferential sections at regular intervals through the left ventricular wall (at 10–90% of the wall thickness from the epicardium). The sections are parallel to the epicardial surface and are displayed separately in figure 1(c). As can be seen, the muscle fibre orientations change with position through the wall; in the equatorial region the predominant muscle fibre direction rotates from about $+50^\circ$ to $+70^\circ$ (sub-epicardial region) to nearly 0° in the mid-wall region to about -50° to -70° (sub-endocardial region) with respect to the circumferential direction of the left ventricle. It should be emphasized that the layers are not in general parallel to the vessel walls, as can be appreciated from figure 1(b) even though it is often assumed in the literature that they are so parallel.

Figure 1(d) is a schematic of the layered organization of myocytes with a fine weave of endomysial collagen surrounding the myocytes and lateral connections, which are 120 to 150 nm long, between adjacent myocytes. In addition, networks of long perimysial fibres span cleavage planes and connect adjacent muscle layers, which are 3–4 cells thick. The perimysial fibres are most likely to be the major structural elements of the extracellular matrix. They are coiled and have a ratio of contour length to end-to-end distance of approximately 1.3 in the unloaded state of the ventricle (MacKenna *et al.*, 1996). Some branching between adjacent layers is evident although in many instances branching is relatively sparse so that the inter-layer separation can be significant. Capillaries with a fairly dense and uniform distribution within the myocardial layers and on their surfaces are also present, as indicated in figure 1(d). Understanding of the transmural variation of the myocardial tissue structure is important since this specific architecture is responsible for the resistance of the heart to bending and twisting during the cardiac cycle.

The layered organization is characterized by a right-handed orthonormal set of basis vectors and an associated orthogonal curvilinear system of coordinates. The local fixed set of (unit) basis vectors consists of the *fibre axis* $\mathbf{f}_0$, which coincides with the muscle fibre orientation, the *sheet axis* $\mathbf{s}_0$ defined to be in the plane of the layer perpendicular to the fibre direction (sometimes referred to as the cross-fibre direction), and the *sheet-normal axis* $\mathbf{n}_0$, defined to be orthogonal to the other two. Figure 1(e), which shows a cube of layered tissue with the local material coordinates (X_1, X_2, X_3), serves as a basis for the proposed geometrical and constitutive model. In what follows we shall use the labels f, s and n to refer to fibre, sheet and normal, respectively. We shall also use the pairs fs, fn and sn to refer to the fibre-sheet, fibre-normal and sheet-normal planes.

(*b*) *Mechanical behaviour of the passive myocardium*

The passive myocardium tissue is an orthotropic material having three mutually orthogonal planes with distinct material responses, as the results of Dokos *et al.* (2002) from *simple shear* tests on passive ventricular myocardium from pig hearts clearly show. This is illustrated in figure 2, which is based on Fig. 6 from the latter paper. It should be noted, however, that the ordering of the labels fn and fs in Fig. 6 of Dokos *et al.* (2002) is inconsistent with the data shown in the other figures in that paper. To correct this we have switched the roles of fs and fn in figure 2 compared with Fig. 6 of Dokos *et al.* (2002). This point is discussed further in §5(d). The tissue exhibits a regionally-dependent and time-dependent, highly nonlinear behaviour with relatively low hysteresis, and also directionally dependent softening as the strain increases. From figure 2 it can be seen that ventricular myocardium is least resistant to simple shear in the fn and sn planes for shear in the f and s directions, respectively (the lowest curve in figure 2 above the positive shear axis). It is most resistant to shear deformations that produce extension of the myocyte (f) axis in the fs and fn planes (the upper two curves for positive shear). Note, however, that for the planes containing the fibre direction the shear responses (fs) and (fn) in the sheet and normal directions are different. Similarly, for the planes containing the sheet direction the responses (sf) and (sn) in the fibre and normal directions are different. On the other hand, the shear responses in the planes containing the normal direction are the same for the considered specimen.

The passive *biaxial* mechanical properties of non-contracting myocardium are described

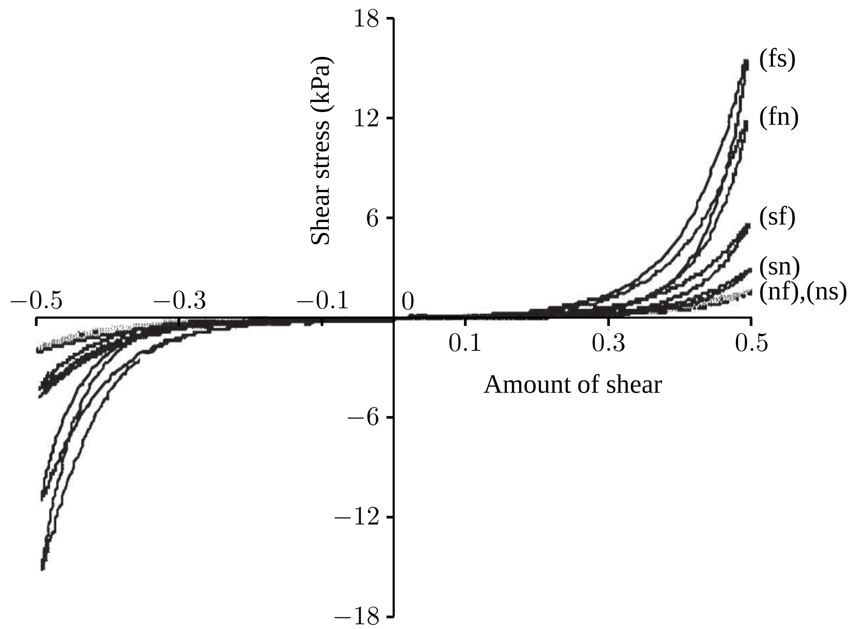

Figure 2. Shear stress versus amount of shear for simple shear tests on a cube of a typical myocardial specimen in the fs, fn and sn planes, where the (ij) shear refers to shear in the j direction in the ij plane, where $i \neq j \in \{\mathrm{f}, \mathrm{s}, \mathrm{n}\}$. Note that the (ij) shear entails stretching of material line elements that are initially in the i direction. The data show clearly the distinct responses for the three planes and hence the orthotropy of the material. In addition, it illustrates the highly nonlinear response and the viscoelastic effect evidenced by the relatively small hysteresis between loading and unloading. For the planes containing the f direction the shear responses (fs) and (fn) in the s and n directions are different; for the planes containing the s direction the responses (sf) and (sn) in the f and n directions are also different; the shear responses (nf) and (ns) in the planes containing the n direction are the same for the considered specimen. Adapted from Dokos *et al.* (2002).

by Demer & Yin (1983), Yin *et al.* (1987), Smaill & Hunter (1991) and Novak *et al.* (1994), for example. To illustrate the results we show in figure 3 representative stress-strain data which we extracted from Fig. 4 in Yin *et al.* (1987). For three different loading protocols for biaxial loading in the fs plane of a canine left ventricle myocardium, figure 3(a) shows the second Piola–Kirchhoff stress S_{ff} in the fibre direction as a function of the Green–Lagrange strain E_{ff} in the same direction, while figure 3(b) shows the corresponding plots for the sheet direction (S_{ss} against E_{ss}). The three sets of data in each of (a) and (b) correspond to constant strain ratios $E_{\mathrm{ff}}/E_{\mathrm{ss}}$. Just as for the shear response the biaxial data indicate high nonlinearity and anisotropy. Data for unloading were not given in Yin *et al.* (1987).

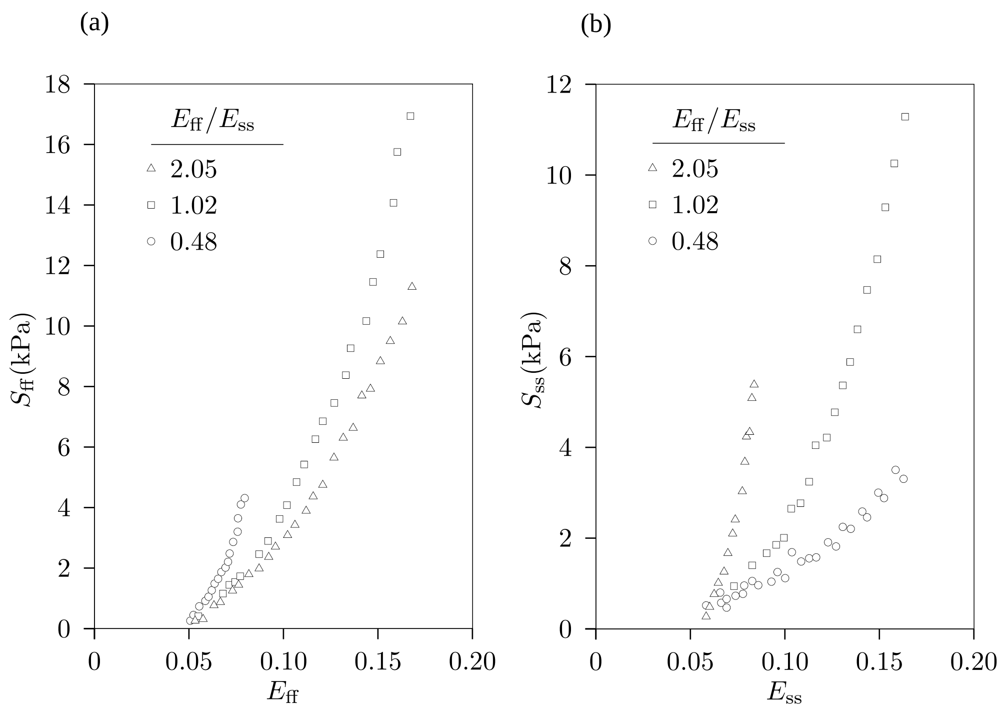

Figure 3. Representative stress-strain data for three different loading protocols for biaxial loading in the fs plane of canine left ventricle myocardium: (a) stress S_{ff} against strain E_{ff} in the fibre direction; (b) stress S_{ss} against strain E_{ss} in the sheet (cross-fibre) direction. Note that E_{ij} and S_{ij} are the components of the Green–Lagrange strain tensor and the second Piola–Kirchhoff stress tensor, respectively. The three sets of data correspond to constant strain ratios E_{ff}/E_{ss} equal to 2.05 (triangles), 1.02 (squares), 0.48 (circles). The data are extracted from the two upper plots in Fig. 4 of Yin *et al.* (1987).

As with many other soft biological tissues, the myocardium can be regarded as an incompressible material. This has been established in experiments by Vossoughi *et al.* (1980), who subjected tissue specimens to various levels of hydrostatic stress. They recorded the associated volumetric strains and concluded that the myocardial tissue is essentially incompressible.

According to experimental data obtained from equatorial slices of the left ventricular wall of potassium arrested rat hearts it is clear that the unloaded myocardium is residually stressed (Omens & Fung, 1990), in particular that there is compressive circumferential residual stress in the endocardium of the left ventricle and tensile circumferential residual stress in the epicardium; see also Costa *et al.* (1997), who suggested that the residual stress in the left ventricle is associated with pre-stretching in the plane of the myocardial sheets. According to Costa *et al.* (1997), there is relatively little residual stress along the muscle fibre direction in the midwall and there are also residual stresses normal to the fibre direction;

the perimysial fibre network may be a primary residual stress bearing structure in passive myocardium. Residual stresses are thought to arise during growth and remodelling (see, for example, Rodriguez *et al.*, 1994 and Rachev, 1997). Residual stresses have an important influence on the stress pattern in the typical physiological state. For example, incorporation of a residual stress distribution may reduce tensile endocardial stress concentrations predicted by ventricular wall models (Guccione *et al.*, 1991). The importance of residual stresses has also been recognized in arterial wall mechanics (see, for example, Holzapfel *et al.*, 2000; Holzapfel & Ogden, 2003). However, three-dimensional residual stresses are very difficult to quantify and hence their modelling must be treated with caution.

Although the myocardium tissue appears to be viscoelastic this aspect of its behaviour is not important from the point of view of mechanical modelling on the time scale of the cardiac cycle, which is short compared with the relaxation time of the viscoelastic response. Indeed, modelling of the viscoelasticity has received little attention in the literature, not least because there are very few data available on the viscoelastic properties of the tissue. An exception to this is the model of Huyghe *et al.* (1991). Here, we treat the tissue behaviour as elastic, with the characteristic features shown in figures 2 and 3.

It is therefore important to model the passive response of the left ventricular myocardium as a non-homogeneous, thick-walled, incompressible, orthotropic nonlinearly elastic material, and this is the approach we adopt in the present paper. Although residual stresses are also important for the stress analysis of the composite myocardium it is first necessary to develop a constitutive model that takes full account of the basic structure of the material with respect to a stress-free reference configuration. Thus, we do not include residual stresses in the constitutive model developed here, as was the case for the arterial model constructed in Holzapfel *et al.* (2000).

3. Essential elements of continuum mechanics

(*a*) *Kinematical quantities and invariants*

The basic deformation variable for the description of the local kinematics is the deformation gradient **F**, and we use the standard notation and convention

$$J = \det \mathbf{F} > 0. \tag{3.1}$$

For an incompressible material we have the constraint

$$J = \det \mathbf{F} \equiv 1. \tag{3.2}$$

Associated with **F** are the right and left Cauchy-Green tensors, defined by

$$\mathbf{C} = \mathbf{F}^{\mathrm{T}}\mathbf{F}, \quad \mathbf{B} = \mathbf{F}\mathbf{F}^{\mathrm{T}}, \tag{3.3}$$

respectively. Also important for what follows is the Green–Lagrange (or Green) strain tensor, defined by

$$\mathbf{E} = \frac{1}{2}(\mathbf{C} - \mathbf{I}), \tag{3.4}$$

where $\mathbf{I}$ is the identity tensor. The principal invariants of $\mathbf{C}$ (also of $\mathbf{B}$) are defined by

$$I_1 = \mathrm{tr}\,\mathbf{C}, \quad I_2 = \frac{1}{2}[I_1^2 - \mathrm{tr}\,(\mathbf{C}^2)], \quad I_3 = \det \mathbf{C}, \tag{3.5}$$

with $I_3 = J^2 = 1$ for an incompressible material. These are *isotropic* invariants. For more details of the relevant material from continuum mechanics we refer to Holzapfel (2000) and Ogden (1997).

If the material has a preferred direction in the reference configuration, denoted by the unit vector $\mathbf{a}_0$, this introduces anisotropy, specifically transverse isotropy, and with it come two additional (transversely isotropic) invariants (or quasi-invariants) defined by

$$I_4 = \mathbf{a}_0 \cdot (\mathbf{C}\mathbf{a}_0), \quad I_5 = \mathbf{a}_0 \cdot (\mathbf{C}^2\mathbf{a}_0). \tag{3.6}$$

Note that these are unaffected by reversal of the direction of $\mathbf{a}_0$. If one wishes to distinguish between the directions $\mathbf{a}_0$ and $-\mathbf{a}_0$ as far as the material response is concerned then yet another invariant would be needed. Here, however, we do not consider this possibility. We refer to Spencer (1984) for background information on the invariant theory of fibre-reinforced materials.

If there are two preferred directions, the second denoted $\mathbf{b}_0$, this introduces the invariants

$$I_6 = \mathbf{b}_0 \cdot (\mathbf{C}\mathbf{b}_0), \quad I_7 = \mathbf{b}_0 \cdot (\mathbf{C}^2\mathbf{b}_0) \tag{3.7}$$

associated with it and, additionally, a coupling invariant, denoted by I_8, which we define here by

$$I_8 = \mathbf{a}_0 \cdot (\mathbf{C}\mathbf{b}_0) = \mathbf{b}_0 \cdot (\mathbf{C}\mathbf{a}_0). \tag{3.8}$$

Note that this changes sign if either $\mathbf{a}_0$ or $\mathbf{b}_0$ (but not both) is reversed and is not therefore strictly invariant in this sense. However, it is more convenient in what follows to use this rather than the strictly invariant form I_8^2 or $I_8\mathbf{a}_0 \cdot \mathbf{b}_0$, and to allow for this distinction in the form of the constitutive law. Note that if $\mathbf{a}_0 \cdot \mathbf{b}_0 = 0$ then only the first of these two options is appropriate, but in this case I_8 depends on $I_1, \ldots, I_7$, specifically

$$I_8^2 = I_2 + I_4 I_6 + I_5 + I_7 - I_1(I_4 + I_6), \tag{3.9}$$

a formula given in Merodio & Ogden (2006). Equation (3.9) determines only the magnitude of I_8 in terms of the other invariants, not its sign.

(*b*) *Strain-energy function and stress tensors*

Here we consider the material properties to be described by a strain-energy function Ψ, which is measured per unit reference volume. This depends on the deformation gradient **F** through **C** (equivalently through **E**), which ensures objectivity. For such an elastic material the Cauchy stress tensor $\boldsymbol{\sigma}$ is given by the formulas

$$J\boldsymbol{\sigma} = \mathbf{F}\frac{\partial\Psi}{\partial\mathbf{F}} = \mathbf{F}\frac{\partial\Psi}{\partial\mathbf{E}}\mathbf{F}^{\mathrm{T}} \tag{3.10}$$

for a compressible material (for Ψ treated as a function of **F** and **E**, respectively), which are modified to

$$\boldsymbol{\sigma} = \mathbf{F}\frac{\partial\Psi}{\partial\mathbf{F}} - p\mathbf{I} = \mathbf{F}\frac{\partial\Psi}{\partial\mathbf{E}}\mathbf{F}^{\mathrm{T}} - p\mathbf{I} \tag{3.11}$$

for an incompressible material, in which case we have the constraint $J = 1$ (equivalently $I_3 = J^2 = 1$) and this is accommodated in the expression for the stress by the Lagrange multiplier p.

For an elastic material possessing a strain-energy function Ψ that depends on a list of invariants, say $I_1, I_2, \ldots, I_N$ for some N, equations (3.10) and (3.11) may be expanded in the forms

$$J\boldsymbol{\sigma} = \mathbf{F}\sum_{i=1}^{N}\psi_i\frac{\partial I_i}{\partial\mathbf{F}}, \qquad \boldsymbol{\sigma} = \mathbf{F}\sum_{i=1, i\neq 3}^{N}\psi_i\frac{\partial I_i}{\partial\mathbf{F}} - p\mathbf{I}, \tag{3.12}$$

respectively, where we have introduced the notation

$$\psi_i = \frac{\partial\Psi}{\partial I_i}, \quad i = 1, 2, \ldots, N, \tag{3.13}$$

with $i = 3$ omitted from the summation for the incompressible material and I_3 omitted from the list of invariants in Ψ in this case. Note that $\partial I_i/\partial\mathbf{F} = (\partial I_i/\partial\mathbf{E})\mathbf{F}^{\mathrm{T}}$ in terms of the Green–Lagrange strain tensor. Note that the second Piola–Kirchhoff stress tensor **S**, whose components were referred to in connection with figure 3, is given in terms of the Cauchy stress tensor via the simple formula $\mathbf{S} = J\mathbf{F}^{-1}\boldsymbol{\sigma}\mathbf{F}^{-\mathrm{T}}$, using (3.10) for a compressible material and (3.11) for an incompressible material with $J = 1$. Explicitly, with **E** as the independent variable, we have simply

$$\mathbf{S} = \frac{\partial\Psi}{\partial\mathbf{E}}, \quad \mathbf{S} = \frac{\partial\Psi}{\partial\mathbf{E}} - p(\mathbf{I} + 2\mathbf{E})^{-1} \tag{3.14}$$

for compressible and incompressible materials, respectively.

4. Review of existing constitutive models

For references to early work concerned with constitutive modelling of the myocardium we refer to papers by Yin (1981) and Humphrey & Yin (1987). Several of the earlier models were based on linear isotropic elasticity, which is entirely inappropriate in view of the discussion in §2(b). Equally, the early nonlinear models do not capture all the features alluded to. This is the case for certain invariant-based models, including the isotropic exponential form based on the invariant I_2 (Demiray, 1976).

(*a*) *Transversely isotropic models*

A number of *transversely isotropic* models have been proposed. These include the model of Humphrey & Yin (1987), which is the sum of two exponentials, one in I_1 and one in I_4, specifically

$$\Psi = c\{\exp[b(I_1 - 3)] - 1\} + A\{\exp[a(\sqrt{I_4} - 1)^2] - 1\}, \tag{4.1}$$

and contains four material parameters, c, b, A, a. This was the first anisotropic invariant-based model that took account of the fibre structure. Another transversely isotropic model, also based on the invariants I_1 and I_4, was constructed by Humphrey *et al.* (1990). This has the form

$$\Psi = c_1(\sqrt{I_4}-1)^2+c_2(\sqrt{I_4}-1)^3+c_3(I_1-3)+c_4(I_1-3)(\sqrt{I_4}-1)+c_5(I_1-3)^2, \tag{4.2}$$

and involves five material constants $c_1, c_2, \ldots, c_5$, values of which were obtained by Novak *et al.* (1994) from biaxial test data from the middle portion of the interventricular septum and the inner, middle and outer layers of the lateral passive canine left ventricle wall. As discussed in §2, it only subsequently became clear that the myocardium is not a transversely isotropic material (see, for example, LeGrice *et al.*, 1995).

The models referred to above are based on the assumption of incompressibility, but the shortcoming referred to above also applies to the compressible transversely isotropic model due to Kerckhoffs *et al.* (2003), which has the form

$$\Psi = a_0[\exp(a_1\hat{I}_1^2 + a_2\hat{I}_2) - 1] + a_3[\exp(a_4E_{\mathrm{ff}}^2) - 1] + a_5(I_3 - 1)^2, \tag{4.3}$$

and contains six material parameters $a_0, a_1, \ldots, a_5$, where $\hat{I}_1$ and $\hat{I}_2$ are the principal invariants of **E** and E_{ff} is the Green–Lagrange strain in the fibre direction. The invariants $\hat{I}_1$ and $\hat{I}_2$ are related to the principal invariants I_1 and I_2 of **C** defined in (3.5) by

$$\hat{I}_1 = \frac{1}{2}(I_1 - 3), \quad \hat{I}_2 = \frac{1}{4}(I_2 - 2I_1 + 3). \tag{4.4}$$

The first term in (4.3) represents the isotropic component related to tissue shape change, the second term relates to the extra stiffness of the material in the myofibre direction, while the third term is related to volume changes.

Other transversely isotropic models, based on use of the components of the Green–Lagrange strain tensor, were developed by Guccione *et al.* (1991) and Costa *et al.* (1996), but again do not reflect the morphology discussed above. They are both special cases of the orthotropic model of Costa *et al.* (2001) to be discussed below.

Some other models are structurally based. These include the model of Horowitz *et al.* (1988), which has the merit of being micro-mechanically motivated and inherently considers possible changes in the waviness of the fibres induced by the tissue strain. On the other hand, because of the integrations involved in the constitutive model, it is not well suited for numerical implementation. It is also effectively transversely isotropic.

The paper by Huyghe *et al.* (1991) contains one of the few models that characterize the passive *viscoelastic* response of the myocardium. It regards the material as sponge-like and treats it as a biphasic (fluid–solid) model based on the quasi-linear viscoelastic constitutive model due to Fung (1993), Section 7.6, and, to our knowledge, is the only biphasic model of the myocardium documented in the literature. The model has been implemented within a finite element framework and applied to the left ventricle of a canine diastolic heart in Huyghe *et al.* (1992). Of interest here is the solid elastic phase, which is a *transversely isotropic* model involving seven material parameters. However, the authors refer to it as *orthotropic*. That it is transversely isotropic can be seen from equation (B8) in Appendix B of Huyghe *et al.* (1992) by noting that their strain-energy function is invariant under interchange of the indices 1 and 2, and hence with respect to rotations about the 3-direction.

(*b*) *Orthotropic models*

Several *orthotropic* models have been proposed in the literature. Some of these are inappropriate for modelling myocardial tissue, including the Langevin eight-chain based model of Bischoff *et al.* (2002), which, as pointed out by Schmid *et al.* (2008), does not reflect the morphology of the myocardium.

In the remainder of this section we describe briefly three orthotropic models that have similar features in that they are partly structurally based, relating to the fibre, sheet and normal directions, and partly phenomenological. This is a prelude to the development, in §5, of a general orthotropic invariant-based model, which includes these three models as special cases.

Note that in the models listed under (i)–(iii) below the authors used the notation E_{ij} with $i, j \in \{\mathrm{f}, \mathrm{s}, \mathrm{n}\}$, and, in particular, although $E_{ij} = E_{ji}$, they expressed the off-diagonal terms in the form $(E_{ij} + E_{ji})/2$, $i \neq j$. Here, for compactness, we simply express this as E_{ij} in each case.

(i) *Strain-energy function proposed by Costa* et al. *(2001)*

The Fung-type exponential strain-energy function due to Costa *et al.* (2001) is given as

$$\Psi = \frac{1}{2}a(\exp Q - 1), \tag{4.5}$$

where

$$Q = b_{\mathrm{ff}}E_{\mathrm{ff}}^2 + b_{\mathrm{ss}}E_{\mathrm{ss}}^2 + b_{\mathrm{nn}}E_{\mathrm{nn}}^2 + 2b_{\mathrm{fs}}E_{\mathrm{fs}}^2 + 2b_{\mathrm{fn}}E_{\mathrm{fn}}^2 + 2b_{\mathrm{sn}}E_{\mathrm{sn}}^2, \tag{4.6}$$

which has seven material parameters, a and $b_{ij},\ i,j \in \{\mathrm{f},\mathrm{s},\mathrm{n}\}$. Interpretations were given for the parameters but specific values were not provided. As already mentioned, transversely isotropic specializations of this model (with 5 material parameters) were used in earlier papers by Guccione *et al.* (1991) and Costa *et al.* (1996).

(ii) *Fung-type model proposed by Schmid* et al. *(2006)*

Another Fung-type model consisting of separate exponential terms for each component E_{ij} was introduced by Schmid *et al.* (2006) in order to decouple the effects of the material parameters in the single exponential model (4.5), (4.6). With 12 material parameters, it is given by

$$\begin{aligned}\Psi \ = \ & \frac{1}{2}a_{\mathrm{ff}}[\exp(b_{\mathrm{ff}}E_{\mathrm{ff}}^2) - 1] + \frac{1}{2}a_{\mathrm{fn}}[\exp(b_{\mathrm{fn}}E_{\mathrm{fn}}^2) - 1] + \frac{1}{2}a_{\mathrm{fs}}[\exp(b_{\mathrm{fs}}E_{\mathrm{fs}}^2) - 1] \\ & + \frac{1}{2}a_{\mathrm{nn}}[\exp(b_{\mathrm{nn}}E_{\mathrm{nn}}^2) - 1] + \frac{1}{2}a_{\mathrm{ns}}[\exp(b_{\mathrm{ns}}E_{\mathrm{ns}}^2) - 1] + \frac{1}{2}a_{\mathrm{s}}[\exp(b_{\mathrm{ss}}E_{\mathrm{ss}}^2) - 1].\end{aligned} \tag{4.7}$$

We mention in passing another model with 12 parameters, which also uses the components $E_{ij},\ i,j \in \{\mathrm{f},\mathrm{s},\mathrm{n}\}$. This is the tangent model introduced in Schmid *et al.* (2006); see also Schmid *et al.* (2008). We do not consider this model here.

(iii) *Pole-zero model proposed by Hunter* et al. *(1997)*

Motivated by the (equi-)biaxial tension tests of Smaill & Hunter (1991), Hunter *et al.* (1997) proposed the so-called *pole-zero* strain-energy function, which has the form

$$\begin{aligned}\Psi \ = \ & \frac{k_{\mathrm{ff}}E_{\mathrm{ff}}^2}{|a_{\mathrm{ff}} - |E_{\mathrm{ff}}||^{b_{\mathrm{ff}}}} + \frac{k_{\mathrm{fn}}E_{\mathrm{fn}}^2}{|a_{\mathrm{fn}} - |E_{\mathrm{fn}}||^{b_{\mathrm{fn}}}} + \frac{k_{\mathrm{nn}}E_{\mathrm{nn}}^2}{|a_{\mathrm{nn}} - |E_{\mathrm{nn}}||^{b_{\mathrm{nn}}}} \\ & + \frac{k_{\mathrm{fs}}E_{\mathrm{fs}}^2}{|a_{\mathrm{fs}} - |E_{\mathrm{fs}}||^{b_{\mathrm{fs}}}} + \frac{k_{\mathrm{ss}}E_{\mathrm{ss}}^2}{|a_{\mathrm{ss}} - |E_{\mathrm{ss}}||^{b_{\mathrm{ss}}}} + \frac{k_{\mathrm{ns}}E_{\mathrm{ns}}^2}{|a_{\mathrm{ns}} - |E_{\mathrm{ns}}||^{b_{\mathrm{ns}}}},\end{aligned} \tag{4.8}$$

with 18 material parameters $k_{ij}, a_{ij}, b_{ij}\ i,j \in \{\mathrm{f},\mathrm{s},\mathrm{n}\}$, and with the different components E_{ij} separated similarly to (4.7). As mentioned in Nash (1998) it was considered unlikely to be suitable for other modes of deformation. Note that several different forms of this model appear in various papers with or without appropriate modulus signs, and in some cases with b_{ij} set equal to 2 for each i,j pair, as in Schmid *et al.* (2006, 2008).

The relative performance of the above orthotropic models in fitting data of Dokos *et al.* (2002) was evaluated in Schmid *et al.* (2008), and we discuss this briefly in §7.

5. A structurally-based model for the passive myocardium

Bearing in mind the fibre, sheet (cross-fibre) and sheet-normal (normal) directions specified in figure 1(e) and the definition of the invariant I_4 in $(3.6)_1$ we now consider the invariant I_4 associated with each of these directions. We use the notations

$$I_{4\,\mathrm{f}} = \mathbf{f}_0 \cdot (\mathbf{C}\mathbf{f}_0), \qquad I_{4\,\mathrm{s}} = \mathbf{s}_0 \cdot (\mathbf{C}\mathbf{s}_0), \qquad I_{4\,\mathrm{n}} = \mathbf{n}_0 \cdot (\mathbf{C}\mathbf{n}_0), \tag{5.1}$$

and note that

$$\sum_{i=\mathrm{f,s,n}} I_{4\,i} = \mathbf{C} : (\mathbf{f}_0 \otimes \mathbf{f}_0 + \mathbf{s}_0 \otimes \mathbf{s}_0 + \mathbf{n}_0 \otimes \mathbf{n}_0) = \mathbf{C} : \mathbf{I} = I_1. \tag{5.2}$$

Thus, only three of the invariants $I_{4\,\mathrm{f}}, I_{4\,\mathrm{s}}, I_{4\,\mathrm{n}}$ and I_1 are independent, and in the functional dependence of the strain energy we may omit one of these.

On the basis of the definition $(3.6)_2$ we may also define invariants $I_{5\,\mathrm{f}}, I_{5\,\mathrm{s}}, I_{5\,\mathrm{n}}$ for each direction. We shall not need these here, but we note that they are related by $I_{5\,\mathrm{f}} + I_{5\,\mathrm{s}} + I_{5\,\mathrm{n}} = I_1^2 - 2I_2$. Additionally, there are the coupling invariants associated with the pairs of directions. In accordance with the definition (3.8) we may write

$$I_{8\,\mathrm{fs}} = I_{8\,\mathrm{sf}} = \mathbf{f}_0 \cdot (\mathbf{C}\mathbf{s}_0), \quad I_{8\,\mathrm{fn}} = I_{8\,\mathrm{nf}} = \mathbf{f}_0 \cdot (\mathbf{C}\mathbf{n}_0), \quad I_{8\,\mathrm{sn}} = I_{8\,\mathrm{ns}} = \mathbf{s}_0 \cdot (\mathbf{C}\mathbf{n}_0). \tag{5.3}$$

In what follows we shall make use of these. In fact, it is not difficult to show that $I_{5\,\mathrm{f}}, I_{5\,\mathrm{s}}, I_{5\,\mathrm{n}}$ are expressible in terms of the other invariants via

$$I_{5\,\mathrm{f}} = I_{4\,\mathrm{f}}^2 + I_{8\,\mathrm{fs}}^2 + I_{8\,\mathrm{fn}}^2, \quad I_{5\,\mathrm{s}} = I_{4\,\mathrm{s}}^2 + I_{8\,\mathrm{fs}}^2 + I_{8\,\mathrm{sn}}^2, \quad I_{5\,\mathrm{n}} = I_{4\,\mathrm{n}}^2 + I_{8\,\mathrm{fn}}^2 + I_{8\,\mathrm{sn}}^2, \tag{5.4}$$

and that

$$I_{4\,\mathrm{f}} I_{4\,\mathrm{s}} I_{4\,\mathrm{n}} - I_{4\,\mathrm{f}} I_{8\,\mathrm{sn}}^2 - I_{4\,\mathrm{s}} I_{8\,\mathrm{fn}}^2 - I_{4\,\mathrm{n}} I_{8\,\mathrm{fs}}^2 + 2 I_{8\,\mathrm{fs}} I_{8\,\mathrm{fn}} I_{8\,\mathrm{sn}} = I_3. \tag{5.5}$$

Thus, if the material is compressible there are seven independent invariants, while for an incompressible material there are six. These numbers compare with the eight (compressible) and seven (incompressible) for the case of a material with two *non-orthogonal* preferred directions. The orthogonality here reduces the number of invariants by one.

Note that in terms of the components $E_{ij},\ i, j \in \{\mathrm{f, s, n}\}$, of the Green–Lagrange strain tensor used in several of the models discussed in §4, we have the connections $2E_{ii} = I_{4\,i} - 1,\ i \in \{\mathrm{f, s, n}\}$ (no summation over i) and $2E_{ij} = I_{8\,ij},\ i \neq j$. Thus, the general framework herein embraces the orthotropic models discussed in §4 as special cases.

Before we consider the most general case we note that for a compressible material that depends only on the invariants I_1, $I_{4\,\mathrm{f}}$, $I_{4\,\mathrm{s}}$, I_3, for example, the formula $(3.12)_1$ yields

$$J\boldsymbol{\sigma} = 2\psi_1\mathbf{B} + 2\psi_{4\,\mathrm{f}}\mathbf{f}\otimes\mathbf{f} + 2\psi_{4\,\mathrm{s}}\mathbf{s}\otimes\mathbf{s} + 2I_3\psi_3\mathbf{I}, \tag{5.6}$$

where $\mathbf{B} = \mathbf{F}\mathbf{F}^{\mathrm{T}}$, $\mathbf{f} = \mathbf{F}\mathbf{f}_0$, $\mathbf{s} = \mathbf{F}\mathbf{s}_0$, and $\psi_{4\,\mathrm{i}} = \partial\Psi/\partial I_{4\,\mathrm{i}}$, $i = \mathrm{f}, \mathrm{s}$. We shall also use the notation $\mathbf{n} = \mathbf{F}\mathbf{n}_0$. The counterpart of the formula (5.6) for an incompressible materials is

$$\boldsymbol{\sigma} = 2\psi_1\mathbf{B} + 2\psi_{4\,\mathrm{f}}\mathbf{f}\otimes\mathbf{f} + 2\psi_{4\,\mathrm{s}}\mathbf{s}\otimes\mathbf{s} - p\mathbf{I}. \tag{5.7}$$

Note that here we have omitted the invariant $I_{4\,\mathrm{n}}$ rather than I_1, $I_{4\,\mathrm{f}}$ or $I_{4\,\mathrm{s}}$. There is a good physical reason for this choice, as we will explain in §6.

(*a*) *Application to simple shear*

Consider now simple shear in different planes and choose the axes so that the component vectors are given by

$$[\mathbf{f}_0] = [1 \quad 0 \quad 0]^{\mathrm{T}}, \quad [\mathbf{s}_0] = [0 \quad 1 \quad 0]^{\mathrm{T}}, \quad [\mathbf{n}_0] = [0 \quad 0 \quad 1]^{\mathrm{T}}. \tag{5.8}$$

We now consider simple shear separately in each of the three planes fs, sn, fn, and we identify the indices $1, 2, 3$ with $\mathrm{f}, \mathrm{s}, \mathrm{n}$, respectively (see figure 4).

(i) *Shear in the* fs *plane*

We begin with simple shear in the fs plane and consider separately shear in the $\mathbf{f}_0$ and the $\mathbf{s}_0$ directions. For shears in the $\mathbf{f}_0$ and the $\mathbf{s}_0$ directions the deformation gradients have components

$$[\mathbf{F}] = \begin{bmatrix} 1 & \gamma & 0 \\ 0 & 1 & 0 \\ 0 & 0 & 1 \end{bmatrix}, \qquad [\mathbf{F}] = \begin{bmatrix} 1 & 0 & 0 \\ \gamma & 1 & 0 \\ 0 & 0 & 1 \end{bmatrix}, \tag{5.9}$$

respectively. For the shear in the $\mathbf{f}_0$ direction we obtain

$$[\mathbf{B}] = \begin{bmatrix} 1+\gamma^2 & \gamma & 0 \\ \gamma & 1 & 0 \\ 0 & 0 & 1 \end{bmatrix}, \qquad \mathbf{f} = \mathbf{f}_0, \qquad \mathbf{s} = \gamma\mathbf{f}_0 + \mathbf{s}_0, \qquad \mathbf{n} = \mathbf{n}_0, \tag{5.10}$$

$I_{4\,\mathrm{s}} = 1 + \gamma^2, I_{4\,\mathrm{f}} = I_{4\,\mathrm{n}} = 1$, the active shear stress is $\sigma_{12} = 2\gamma(\psi_1 + \psi_{4\,\mathrm{s}})$, and $\sigma_{13} = \sigma_{23} = 0$.

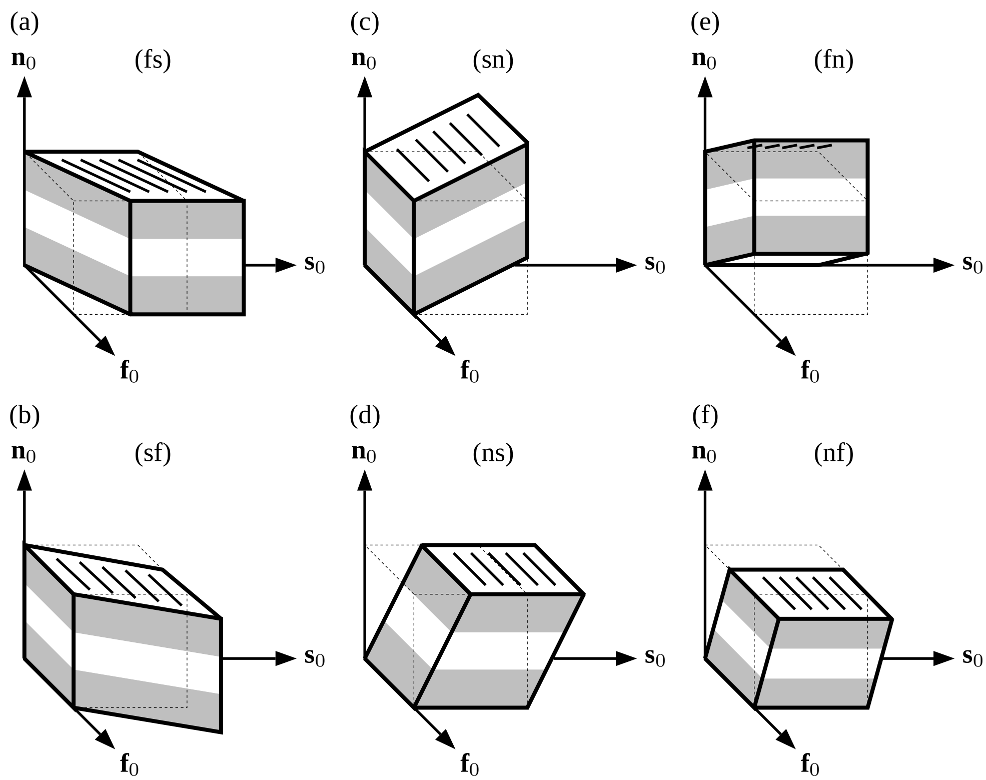

Figure 4. Sketches (a)–(f) of six possible modes of simple shear for myocardium defined with respect to the fibre axis $\mathbf{f}_0$, sheet axis $\mathbf{s}_0$, and sheet-normal axis, $\mathbf{n}_0$: each mode is a plane strain deformation. The modes are designated (ij), $i, j \in \{\mathrm{f}, \mathrm{s}, \mathrm{n}\}$, corresponding to shear in the ij plane with shear in the j direction. Thus, the first letter in (ij) denotes the normal vector of the face that is shifted by the simple shear, while the second denotes the direction in which that face is shifted. The modes in which the fibres are stretched are (fn) and (fs).

For the shear in the $\mathbf{s}_0$ direction we have

$$[\mathbf{B}] = \begin{bmatrix} 1 & \gamma & 0 \\ \gamma & 1+\gamma^2 & 0 \\ 0 & 0 & 1 \end{bmatrix}, \qquad \mathbf{f} = \mathbf{f}_0 + \gamma \mathbf{s}_0, \qquad \mathbf{s} = \mathbf{s}_0, \qquad \mathbf{n} = \mathbf{n}_0, \quad (5.11)$$

$I_{4\,\mathrm{f}} = 1 + \gamma^2, I_{4\,\mathrm{s}} = I_{4\,\mathrm{n}} = 1$, the active shear stress is $\sigma_{12} = 2\gamma(\psi_1 + \psi_{4\,\mathrm{f}})$, and again $\sigma_{13} = \sigma_{23} = 0$. Hence, the two shear responses in the fs plane are different. Note that for each of the above two cases $I_{8\,\mathrm{fs}} = \gamma$ and $I_{8\,\mathrm{fn}} = I_{8\,\mathrm{sn}} = 0$.

(ii) *Shear in the* sn *plane*

Next, we consider simple shear in the sn plane, considering separately shear in the $\mathbf{s}_0$ and $\mathbf{n}_0$ directions. Shears in the $\mathbf{s}_0$ and the $\mathbf{n}_0$ directions have deformation gradients with components

$$[\mathbf{F}] = \begin{bmatrix} 1 & 0 & 0 \\ 0 & 1 & \gamma \\ 0 & 0 & 1 \end{bmatrix}, \qquad [\mathbf{F}] = \begin{bmatrix} 1 & 0 & 0 \\ 0 & 1 & 0 \\ 0 & \gamma & 1 \end{bmatrix}, \tag{5.12}$$

respectively. For the shear in the $\mathbf{s}_0$ direction we have

$$[\mathbf{B}] = \begin{bmatrix} 1 & 0 & 0 \\ 0 & 1+\gamma^2 & \gamma \\ 0 & \gamma & 1 \end{bmatrix}, \qquad \mathbf{f} = \mathbf{f}_0, \qquad \mathbf{s} = \mathbf{s}_0, \qquad \mathbf{n} = \mathbf{n}_0 + \gamma\mathbf{s}_0, \tag{5.13}$$

$I_{4\,\mathrm{n}} = 1+\gamma^2, I_{4\,\mathrm{f}} = I_{4\,\mathrm{s}} = 1$, the active shear stress is $\sigma_{23} = 2\gamma\psi_1$, and $\sigma_{12} = \sigma_{13} = 0$.

For the shear in the $\mathbf{n}_0$ direction we obtain

$$[\mathbf{B}] = \begin{bmatrix} 1 & 0 & 0 \\ 0 & 1 & \gamma \\ 0 & \gamma & 1+\gamma^2 \end{bmatrix}, \qquad \mathbf{f} = \mathbf{f}_0, \qquad \mathbf{s} = \mathbf{s}_0 + \gamma\mathbf{n}_0, \qquad \mathbf{n} = \mathbf{n}_0, \tag{5.14}$$

$I_{4\,\mathrm{s}} = 1+\gamma^2, I_{4\,\mathrm{f}} = I_{4\,\mathrm{n}} = 1$, the active shear stress is $\sigma_{23} = 2\gamma(\psi_1 + \psi_{4\,\mathrm{s}})$, and $\sigma_{12} = \sigma_{13} = 0$. Hence, the two shear responses in the sn plane are different. Note that for each of the above two cases $I_{8\,\mathrm{sn}} = \gamma$ and $I_{8\,\mathrm{fs}} = I_{8\,\mathrm{fn}} = 0$.

(iii) *Shear in the* fn *plane*

Finally, we have simple shear in the fn plane. For shears in the $\mathbf{f}_0$ and $\mathbf{n}_0$ directions the deformation gradients are

$$[\mathbf{F}] = \begin{bmatrix} 1 & 0 & \gamma \\ 0 & 1 & 0 \\ 0 & 0 & 1 \end{bmatrix}, \qquad [\mathbf{F}] = \begin{bmatrix} 1 & 0 & 0 \\ 0 & 1 & 0 \\ \gamma & 0 & 1 \end{bmatrix}, \tag{5.15}$$

respectively. For the shear in the $\mathbf{f}_0$ direction we have

$$[\mathbf{B}] = \begin{bmatrix} 1+\gamma^2 & 0 & \gamma \\ 0 & 1 & 0 \\ \gamma & 0 & 1 \end{bmatrix}, \qquad \mathbf{f} = \mathbf{f}_0, \qquad \mathbf{s} = \mathbf{s}_0, \qquad \mathbf{n} = \mathbf{n}_0 + \gamma\mathbf{f}_0, \tag{5.16}$$

$I_{4\,\mathrm{n}} = 1+\gamma^2, I_{4\,\mathrm{f}} = I_{4\,\mathrm{s}} = 1$, the active shear stress is $\sigma_{13} = 2\gamma\psi_1$, and $\sigma_{12} = \sigma_{23} = 0$.

For the shear in the $\mathbf{n}_0$ direction we have

$$[\mathbf{B}] = \begin{bmatrix} 1 & 0 & \gamma \\ 0 & 1 & 0 \\ \gamma & 0 & 1+\gamma^2 \end{bmatrix}, \qquad \mathbf{f} = \mathbf{f}_0 + \gamma\mathbf{n}_0, \qquad \mathbf{s} = \mathbf{s}_0, \qquad \mathbf{n} = \mathbf{n}_0, \tag{5.17}$$

$I_{4\,\mathrm{f}} = 1+\gamma^2, I_{4\,\mathrm{s}} = I_{4\,\mathrm{n}} = 1$, the active shear stress is $\sigma_{13} = 2\gamma(\psi_1 + \psi_{4\,\mathrm{f}})$, and $\sigma_{12} = \sigma_{23} = 0$. Hence, the two shear responses in the fn plane are different. Note that for each of the above two cases $I_{8\,\mathrm{fn}} = \gamma$ and $I_{8\,\mathrm{fs}} = I_{8\,\mathrm{sn}} = 0$.

Clearly, the (nf) and (ns) shear responses are the same, where we now recall that we use the notation (ij) to specify that the shear is in the j direction in the ij plane, with $i, j \in \{\mathrm{f}, \mathrm{s}, \mathrm{n}\}$. In these two cases there is stretching along the $\mathbf{n}_0$ direction but not along the $\mathbf{f}_0$ or $\mathbf{s}_0$ directions. The (sn) and (sf) shear responses are also the same, with no stretching along the $\mathbf{f}_0$ or $\mathbf{n}_0$ directions, and, finally, the responses are also the same in the fs and fn planes, with stretching along the fibre direction $\mathbf{f}_0$ in these cases. It should be emphasized that in the above the order of the indices i and j in (ij) (when referring to *shear* or *response*) is important, but without parenthesis, in ij, the order is not relevant (when referring to *plane*).

The data of Dokos *et al.* (2002) indicate that the shear response is stiffest when the fibre direction is extended, least stiff when the normal direction is extended and has intermediate stiffness when the sheet direction is extended. This is reflected by the above formulas for the shear stresses if $\psi_{4\,\mathrm{f}} > \psi_{4\,\mathrm{s}} > 0$. However, the data also show that there are differences between the (fs) and (fn) and between the (sf) and (sn) responses, which are not captured by the above model; the data show also that the (nf) and (ns) responses are indistinguishable. A possible way to refine the model in order to reflect these differences is to include in the strain-energy function one or more of the coupling invariants defined in (5.3). Bearing in mind that the most general strain-energy function depends only on seven invariants for a compressible material we may select, for example, $I_1, I_2, I_3, I_{4\,\mathrm{f}}, I_{4\,\mathrm{s}}, I_{8\,\mathrm{fs}}, I_{8\,\mathrm{fn}}$, in which case the Cauchy stress (5.6) is given by

$$\begin{aligned} J\boldsymbol{\sigma} = {} & 2\psi_1\mathbf{B} + 2\psi_2(I_1\mathbf{B} - \mathbf{B}^2) + 2I_3\psi_3\mathbf{I} + 2\psi_{4\,\mathrm{f}}\mathbf{f}\otimes\mathbf{f} + 2\psi_{4\,\mathrm{s}}\mathbf{s}\otimes\mathbf{s} \\ & + \psi_{8\,\mathrm{fs}}(\mathbf{f}\otimes\mathbf{s} + \mathbf{s}\otimes\mathbf{f}) + \psi_{8\,\mathrm{fn}}(\mathbf{f}\otimes\mathbf{n} + \mathbf{n}\otimes\mathbf{f}). \end{aligned} \tag{5.18}$$

We emphasize that the invariants $I_{8\,\mathrm{fs}}$ and $I_{8\,\mathrm{fn}}$ appearing in (5.18), and also $I_{8\,\mathrm{sn}}$, depend on the *sense* of $\mathbf{f}_0$, $\mathbf{s}_0$ and $\mathbf{n}_0$, i.e. they change sign if the sense of one of the vectors is reversed. However, Ψ should be independent of this sense and this is accommodated by an appropriate functional dependence. For example, if we write $\hat{\Psi}(..., I_{8\,\mathrm{fs}}^2, ...) = \Psi(..., I_{8\,\mathrm{fs}}, ...)$ then $\psi_{8\,\mathrm{fs}} = 2\partial\hat{\Psi}/\partial(I_{8\,\mathrm{fs}}^2)I_{8\,\mathrm{fs}}$ and for shear in the fs plane we have $I_{8\,\mathrm{fs}} = \mathbf{f}\cdot\mathbf{s} = \gamma$ for either direction of shear, and this vanishes in the reference configuration, as does $\psi_{8\,\mathrm{fs}}$ provided Ψ is well behaved as a function of $I_{8\,\mathrm{fs}}^2$ (which we assume to be the case). Similarly, $I_{8\,\mathrm{fn}} = \mathbf{f}\cdot\mathbf{n} = \gamma$ for shear in the fn plane and $I_{8\,\mathrm{sn}} = \mathbf{s}\cdot\mathbf{n} = \gamma$ for shear in the sn plane.

In view of the above, in the reference configuration equation (5.18) reduces to

$$2(\psi_1 + 2\psi_2 + \psi_3)\mathbf{I} + 2\psi_{4\,\mathrm{f}}\mathbf{f}_0 \otimes \mathbf{f}_0 + 2\psi_{4\,\mathrm{s}}\mathbf{s}_0 \otimes \mathbf{s}_0 = \mathbf{0}, \tag{5.19}$$

assuming the reference configuration is stress free, and this can only hold if

$$\psi_1 + 2\psi_2 + \psi_3 = 0, \quad \psi_{4\,\mathrm{f}} = 0, \quad \psi_{4\,\mathrm{s}} = 0. \tag{5.20}$$

Thus, these conditions must be satisfied along with

$$\psi_{8\,\mathrm{fs}} = \psi_{8\,\mathrm{fn}} = 0 \tag{5.21}$$

in the reference configuration.

For an incompressible material (5.18) is replaced by

$$\begin{aligned}\boldsymbol{\sigma} = 2\psi_1\mathbf{B} + 2\psi_2(I_1\mathbf{B} - \mathbf{B}^2) - p\mathbf{I} + 2\psi_{4\,\mathrm{f}}\mathbf{f}\otimes\mathbf{f} + 2\psi_{4\,\mathrm{s}}\mathbf{s}\otimes\mathbf{s}\\ + \psi_{8\,\mathrm{fs}}(\mathbf{f}\otimes\mathbf{s} + \mathbf{s}\otimes\mathbf{f}) + \psi_{8\,\mathrm{fn}}(\mathbf{f}\otimes\mathbf{n} + \mathbf{n}\otimes\mathbf{f}),\end{aligned} \tag{5.22}$$

and only the six invariants $I_1, I_2, I_{4\,\mathrm{f}}, I_{4\,\mathrm{s}}, I_{8\,\mathrm{fs}}, I_{8\,\mathrm{fn}}$ remain. In this case, the conditions that must be satisfied in the reference configuration are as above except for the first in (5.20), which is replaced by $2\psi_1 + 4\psi_2 - p_0 = 0$, where p_0 is the value of p in the reference configuration.

For simple shear in the fs plane the term in $\psi_{8\,\mathrm{fs}}$ contributes $\psi_{8\,\mathrm{fs}}$ to σ_{12} for shear in either the $\mathbf{f}_0$ or $\mathbf{s}_0$ direction but does not contribute if the shear is in either the fn or the sn plane. The term in $\psi_{8\,\mathrm{fn}}$ similarly contributes $\psi_{8\,\mathrm{fn}}$ to σ_{13} for shear in either the $\mathbf{f}_0$ or $\mathbf{n}_0$ direction in the fn plane. And since, as noted above, the dependence of Ψ is on the square of each of these invariants these two terms each involve a factor of γ.

In summary, the shear stress versus amount of shear equations for the six simple shears enumerated in (i)–(iii) are given by

$$\text{(fs):}\quad \sigma_{\mathrm{fs}} = 2(\psi_1 + \psi_2 + \psi_{4\,\mathrm{f}})\gamma + \psi_{8\,\mathrm{fs}}, \tag{5.23}$$

$$\text{(fn):}\quad \sigma_{\mathrm{fn}} = 2(\psi_1 + \psi_2 + \psi_{4\,\mathrm{f}})\gamma + \psi_{8\,\mathrm{fn}}, \tag{5.24}$$

$$\text{(sf):}\quad \sigma_{\mathrm{fs}} = 2(\psi_1 + \psi_2 + \psi_{4\,\mathrm{s}})\gamma + \psi_{8\,\mathrm{fs}}, \tag{5.25}$$

$$\text{(sn):}\quad \sigma_{\mathrm{sn}} = 2(\psi_1 + \psi_2 + \psi_{4\,\mathrm{s}})\gamma, \tag{5.26}$$

$$\text{(nf):}\quad \sigma_{\mathrm{fn}} = 2(\psi_1 + \psi_2)\gamma + \psi_{8\,\mathrm{fn}}, \tag{5.27}$$

$$\text{(ns):}\quad \sigma_{\mathrm{sn}} = 2(\psi_1 + \psi_2)\gamma. \tag{5.28}$$

It is worth remarking here that since simple shear is a plane strain deformation the invariants I_1 and I_2 are identical and the effects of ψ_1 and ψ_2 cannot be distinguished.

(*b*) *Application to biaxial deformation*

Several experiments have been conducted using biaxial tests on thin sheets of tissue taken from planes parallel to the endocardium. Such specimens are purportedly from within a sheet containing the fibre axis and the in-sheet axis. These are referred to as the fibre and cross-fibre directions. Note, however, that according to the structure discussed in §2, such specimens are in general unlikely to contain a specific myocyte sheet, so care must be exercised in interpreting such biaxial data.

Consider the pure homogeneous deformation defined by

$$x_1 = \lambda_{\rm f} X_1, \quad x_2 = \lambda_{\rm s} X_2, \quad x_3 = \lambda_{\rm n} X_3, \tag{5.29}$$

where $\lambda_{\rm f}, \lambda_{\rm s}, \lambda_{\rm n}$ are the principal stretches, identified with the fibre, sheet and normal directions, respectively. They satisfy the incompressibility condition

$$\lambda_{\rm f}\lambda_{\rm s}\lambda_{\rm n} = 1. \tag{5.30}$$

When the deformation (5.29) is applied to a thin sheet of tissue parallel to a sheet with no lateral stress there is no shear strain and hence $I_{8\,ij} = 0,\ i \neq j \in \{\rm f, s, n\}$, and $\psi_{8\,ij} = 0$ correspondingly. Equation (5.22) then has only three components, namely

$$\begin{aligned}
\sigma_{\rm ff} &= 2\psi_1\lambda_{\rm f}^2 + 2\psi_2(\lambda_{\rm s}^2 + \lambda_{\rm n}^2)\lambda_{\rm f}^2 + 2\psi_{4\,\rm f}\lambda_{\rm f}^2 - p, && (5.31)\\
\sigma_{\rm ss} &= 2\psi_1\lambda_{\rm s}^2 + 2\psi_2(\lambda_{\rm n}^2 + \lambda_{\rm f}^2)\lambda_{\rm s}^2 + 2\psi_{4\,\rm s}\lambda_{\rm s}^2 - p, && (5.32)\\
0 &= 2\psi_1\lambda_{\rm n}^2 + 2\psi_2(\lambda_{\rm f}^2 + \lambda_{\rm s}^2)\lambda_{\rm n}^2 - p. && (5.33)
\end{aligned}$$

Elimination of p by means of (5.33) allows (5.31) and (5.32) to be expressed as

$$\begin{aligned}
\sigma_{\rm ff} &= 2\psi_1(\lambda_{\rm f}^2 - \lambda_{\rm n}^2) + 2\psi_2\lambda_{\rm s}^2(\lambda_{\rm f}^2 - \lambda_{\rm n}^2) + 2\psi_{4\,\rm f}\lambda_{\rm f}^2, && (5.34)\\
\sigma_{\rm ss} &= 2\psi_1(\lambda_{\rm s}^2 - \lambda_{\rm n}^2) + 2\psi_2\lambda_{\rm f}^2(\lambda_{\rm s}^2 - \lambda_{\rm n}^2) + 2\psi_{4\,\rm s}\lambda_{\rm s}^2. && (5.35)
\end{aligned}$$

If we omit the dependence on the invariant I_2 then the latter two equations simplify to

$$\begin{aligned}
\sigma_{\rm ff} &= 2\psi_1(\lambda_{\rm f}^2 - \lambda_{\rm n}^2) + 2\psi_{4\,\rm f}\lambda_{\rm f}^2, && (5.36)\\
\sigma_{\rm ss} &= 2\psi_1(\lambda_{\rm s}^2 - \lambda_{\rm n}^2) + 2\psi_{4\,\rm s}\lambda_{\rm s}^2. && (5.37)
\end{aligned}$$

(*c*) *A specific model*

In order to decide which of the invariants to include in a particular model we now examine interpretations of the invariants. First, we include an isotropic term based on the invariant I_1 since this can be regarded as associated with the underlying non-collagenous and non-muscular matrix (which includes fluids). This could be modelled as a neo-Hookean

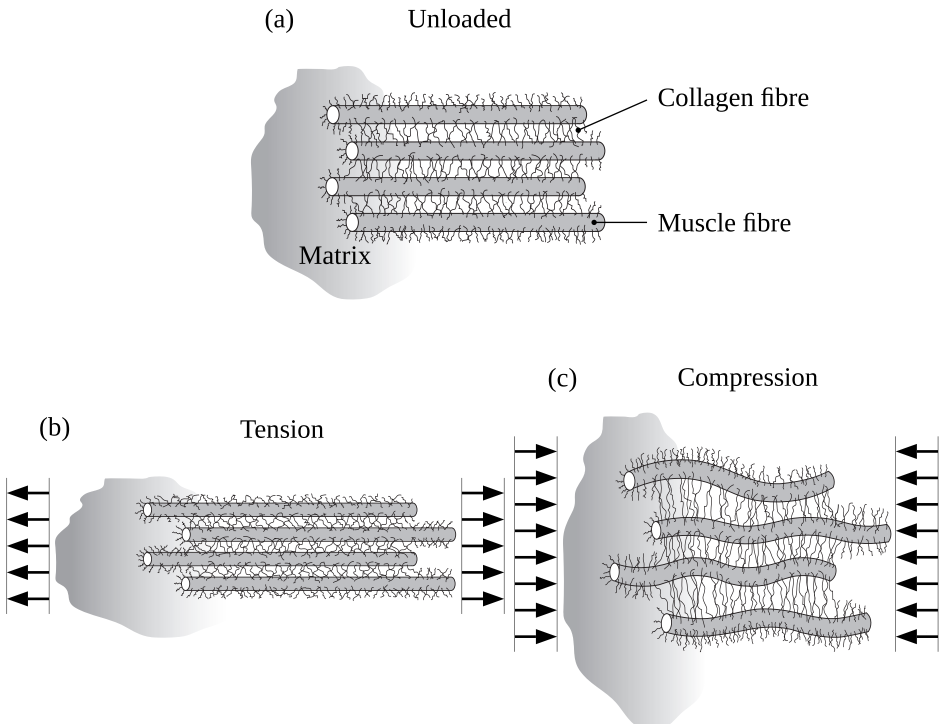

Figure 5. Schematic representation of the arrangement of muscle and collagen fibres and the surrounding matrix: (a) unloaded structure; (b) structure under tensile load in the muscle fibre direction, showing decreased inter-fibre separation so that the collagen network bears load primarily in the muscle fibre direction; (c) structure under compressive load in the muscle fibre direction, showing the muscle fibres buckled and lateral extension of the collagen network.

material, as in the case of arteries (Holzapfel *et al.*, 2000), or as an exponential (Demiray, 1972), for example.

A schematic of the embedded collagen-muscle fibre structure is shown in figure 5 for the unloaded configuration and, separately, for configurations subject to tension and compression in the direction of the muscle fibre (cardiac myocyte). The collagen fibres illustrated in figure 5 are thought to represent both the endomysial and the perimysial collagen fibres, as briefly described in §2(a). Figure 5(b), in particular, shows the configuration in which the tensile loading is in the muscle fibre direction. The muscle fibres are extended and the inter-fibre distances are decreased while the collagenous network offers little resistance laterally but does contribute to the exponentially increasing stress in the muscle fibre direction. For tensile loading lateral to the muscle fibres there is also exponential stress stiffening, which can be thought as being generated by recruitment of the collagen network. Figure 5(c) depicts the tendency of the muscle fibres to buckle under compressive load in the muscle fibre direction and stretched collagen cross fibres, i.e. the lateral inter-fibre connections as well as the woven perimysial network are stretched. It is suggested that the lateral stretching of the collagen fibres contributes to the observed relatively high compressive stiffness of the myocardium.

To reflect the stiffening behaviour in the muscle fibre direction, as shown by experimental tests (see, for example, figures 2 and 3) it is appropriate to use an exponential function of $I_{4\,\mathrm{f}}$. Similarly, for the sheet direction transverse to the muscle fibres; in this direction the stiffening is in part associated with the collagen fibres connecting the muscle fibres, as discussed above. For this direction we use an exponential function of the invariant $I_{4\,\mathrm{s}}$. Clearly, these terms contribute significantly to the stored energy when the associated directions are under tension. However, when they are under compression their contribution is minimal since the fibres do not support compression. For this reason we include these terms in the energy function only if $I_{4\,\mathrm{f}} > 1$ or $I_{4\,\mathrm{s}} > 1$, as appropriate. Since $I_{4\,\mathrm{n}}$ depends on I_1, $I_{4\,\mathrm{f}}$ and $I_{4\,\mathrm{s}}$ we do not include it separately and therefore tensile and compressive behaviour in the normal direction is accommodated by the term in I_1. These three invariants are sufficient to model the tension/compression behaviour, and there is no need to include I_2. Indeed, they are also sufficient to characterize the basic features of the shear test results of Dokos *et al.* (2002), which we will demonstrate in the following subsection.

As far as the more detailed shear behaviour is concerned (see figure 2) it is necessary to make use of one or more of the invariants $I_{8\,ij}$. In view of the exponential trends shown in figure 2, particularly for the curves (fs) and (fn), we choose to use an exponential function also for this part of the characterization. In particular, since the (nf) and (ns) curves are not distinguished (see figure 2) it turns out that we need consider only the invariant $I_{8\,\mathrm{fs}}$ associated with stretching of the fibres, and not $I_{8\,\mathrm{fn}}$ or $I_{8\,\mathrm{sn}}$. The above considerations lead us to propose the energy function given by

$$\Psi = \frac{a}{2b}\exp[b(I_1-3)] + \sum_{i=\mathrm{f,s}} \frac{a_i}{2b_i}\left\{\exp[b_i(I_{4\,i}-1)^2]-1\right\} + \frac{a_{\mathrm{fs}}}{2b_{\mathrm{fs}}}\left[\exp(b_{\mathrm{fs}}I_{8\,\mathrm{fs}}^2)-1\right], \tag{5.38}$$

where $a, b, a_{\mathrm{f}}, a_{\mathrm{s}}, b_{\mathrm{f}}, b_{\mathrm{s}}, a_{\mathrm{fs}}, b_{\mathrm{fs}}$ are eight positive material constants, the a parameters having dimension of stress while the b parameters are dimensionless. This consists of the isotropic term in I_1, the transversely isotropic terms in $I_{4\,\mathrm{f}}$ and $I_{4\,\mathrm{s}}$ and the orthotropic term in $I_{8\,\mathrm{fs}}$. Note that if we do not distinguish between the (fs) and (fn) and between the (sf) and (sn) responses then only six constants are needed.

From equation (5.22) this yields the Cauchy stress

$$\begin{aligned}\boldsymbol{\sigma} \;=\; & a\exp[b(I_1-3)]\mathbf{B}-p\mathbf{I}+2a_{\mathrm{f}}(I_{4\,\mathrm{f}}-1)\exp[b_{\mathrm{f}}(I_{4\,\mathrm{f}}-1)^2]\mathbf{f}\otimes\mathbf{f}\\ & +2a_{\mathrm{s}}(I_{4\,\mathrm{s}}-1)\exp[b_{\mathrm{s}}(I_{4\,\mathrm{s}}-1)^2]\mathbf{s}\otimes\mathbf{s}+a_{\mathrm{fs}}I_{8\,\mathrm{fs}}\exp(b_{\mathrm{fs}}I_{8\,\mathrm{fs}}^2)(\mathbf{f}\otimes\mathbf{s}+\mathbf{s}\otimes\mathbf{f}).\end{aligned} \tag{5.39}$$

In the following subsection we apply this specific strain-energy function to both biaxial and shear test data and discuss the results in detail.

(*d*) *Fit of the Yin* et al. *(1987) and Dokos* et al. *(2002) data*

In this subsection we show the efficacy of the proposed model for fitting data on the myocardium. First, we use the simplified model based on the three invariants $I_1, I_{4\,\mathrm{f}}, I_{4\,\mathrm{s}}$ for which the Cauchy stress is given by (5.39) with the final term omitted. The resulting fit with the mean of the loading curves for positive (fs) and (fn) and for positive (sf) and (sn) shears, as well as the common curve for positive (nf) and (ns) shears, extracted from figure 2, is shown in figure 6. Clearly, this simple model reflects the general characteristics of the distinct shears in the different directions, which exemplify the orthotropy. It is also worth noting that if the isotropic term is replaced by the neo-Hookean term $\mu(I_1-3)/2$ the fit is still relatively good, although the shear stress versus amount of shear is then linear for the (nf)–(ns) plot. We do not show this plot. The data shown in figure 2 indicate that the response for negative shears is very similar to that for positive shear (with reversed sign of the amount of shear and shear stress). Fitting the negative shear data along with those for positive shear would have a minor effect on the values of the fitting parameters.

Second, with this as a starting point we now refine the fitting by including the final term in (5.39) which allows the (fs) and (fn) and the (sf) and (sn) plots to be separated according to figure 2. The resulting fit is shown in figure 7 and indicates very good agreement between the model and the experimental data. As mentioned in §2(b), we have reversed the labels fn and fs compared with those in Dokos *et al.* (2002). This is because all the other curves in the latter paper show that the (fs) shear response is stiffer than that for (fn). This indeed makes sense since the stiffnesses in the f, s and n directions are, as noted previously, ordered according to f $>$ s $>$ n. Thus, the (fs) shear response is expected to be stiffer than the (fn) response. Equally, the (sf) response is stiffer than the (sn) response. It is also suggested that the (nf) response should be stiffer than the (ns) response, although there is no clear distinction seen in figure 2. Other data shown in Dokos *et al.* (2002) do indeed show a small separation in the sense just indicated. The values of the material parameters for the fits shown in figures 6 and 7 are summarized in table 1.

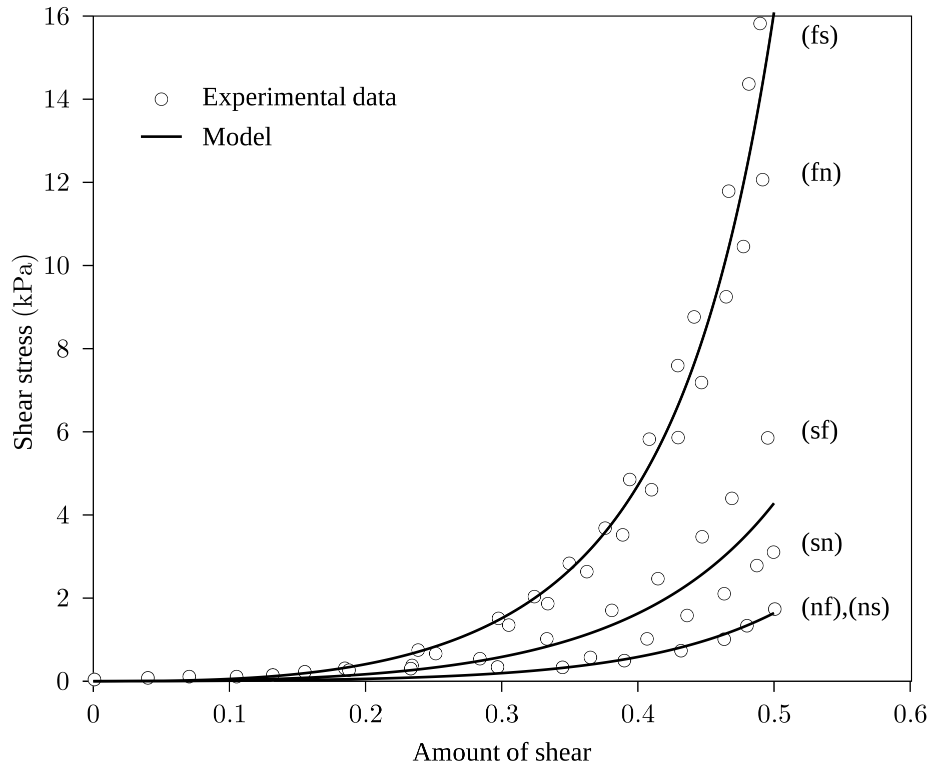

Figure 6. Fit of the model (5.39) with the final term omitted to the experimental data for the loading curves from figure 2: (nf)–(ns) and mean of the loading curves for (fs) and (fn) and for (sf) and (sn). The material parameters used are given in table 1.

Next, we use the model (5.39), specialized for the biaxial mode of deformation according to equations (5.36) and (5.37), to fit the experimental data obtained from Yin *et al.* (1987) and shown in figure 8. The associated material parameters are summarized in the last row of table 1.

We are using here the biaxial data of Yin *et al.* (1987) for illustration purposes since, to our knowledge, they are the only true biaxial, as distinct from equibiaxial, data available. However, these data have limitations, and in, particular, it should be noted that they do not provide information in the low strain region (between 0 and 0.05). This highlights the need for more complete biaxial data. The fit presented in figure 8 is therefore rather crude but can be improved if required by changing the isotropic term, i.e. the I_1 function, and/or by including an activation threshold to accommodate the 'toe' region. Whether or not this is done it is important to recognize that the biaxial data of Yin *et al.* (1987) can be captured by a transversely isotropic specialization of the model. For the model used here, as can be seen from table 1, only four material constants (with $a_{\rm s} = 0$) are required. Hence, the biaxial data alone appear to suggest that the material is transversely isotropic. Since

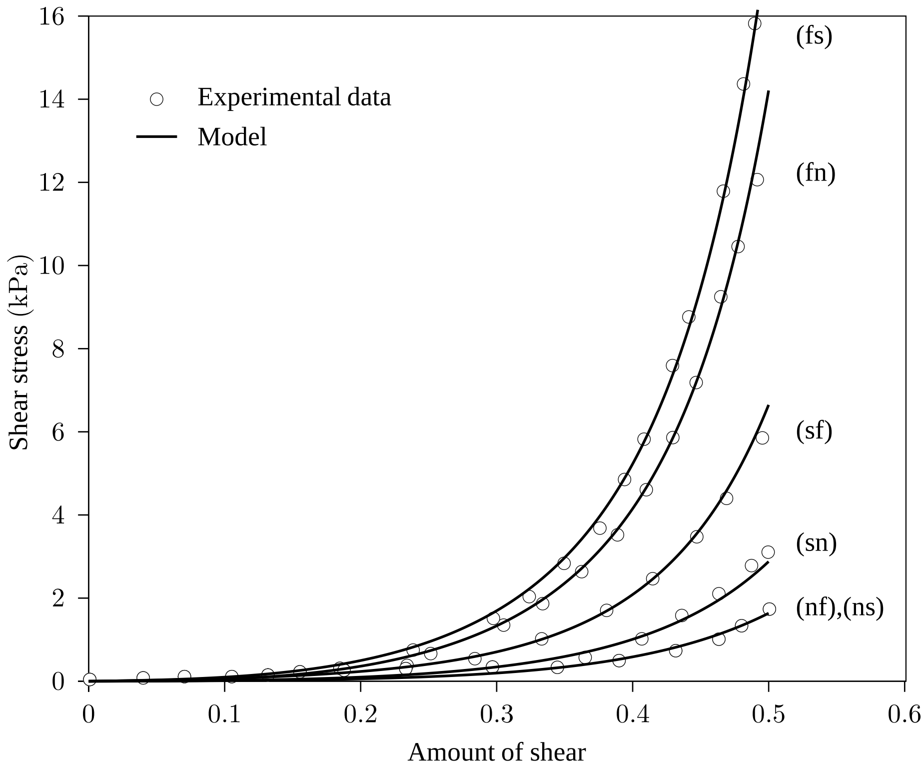

Figure 7. Fit of the model (5.39) to the experimental data for the loading curves from figure 2 with separate (fs), (fn), (sf), (sn), and (nf)–(ns) not distinguished. The material parameters used are given in table 1.

Table 1. Material parameters a, b, a_{f}, b_{f}, a_{s}, b_{s}, a_{fs}, b_{fs} for the energy function (5.38) used to fit the simple shear data for myocardium (Dokos *et al.*, 2002) in figures 6 and 7 and the biaxial tension data (Yin *et al.*, 1987) in figure 8.

Experimental data	a (kPa)	b (-)	a_{f} (kPa)	b_{f} (-)	a_{s} (kPa)	b_{s} (-)	a_{fs} (kPa)	b_{fs} (-)
Shear, Fig. 6	0.057	8.094	21.503	15.819	6.841	6.959	–	–
Shear, Fig. 7	0.059	8.023	18.472	16.026	2.481	11.120	0.216	11.436
Biaxial, Fig. 8	2.280	9.726	1.685	15.779	–	–	–	–

this conflicts sharply with the shear data, care must be taken in drawing conclusions from biaxial data alone. Additional experimental tests are required. For a fuller discussion of the theory underpinning planar biaxial tests for anisotropic nonlinearly elastic solids we refer to Holzapfel & Ogden (2009b).

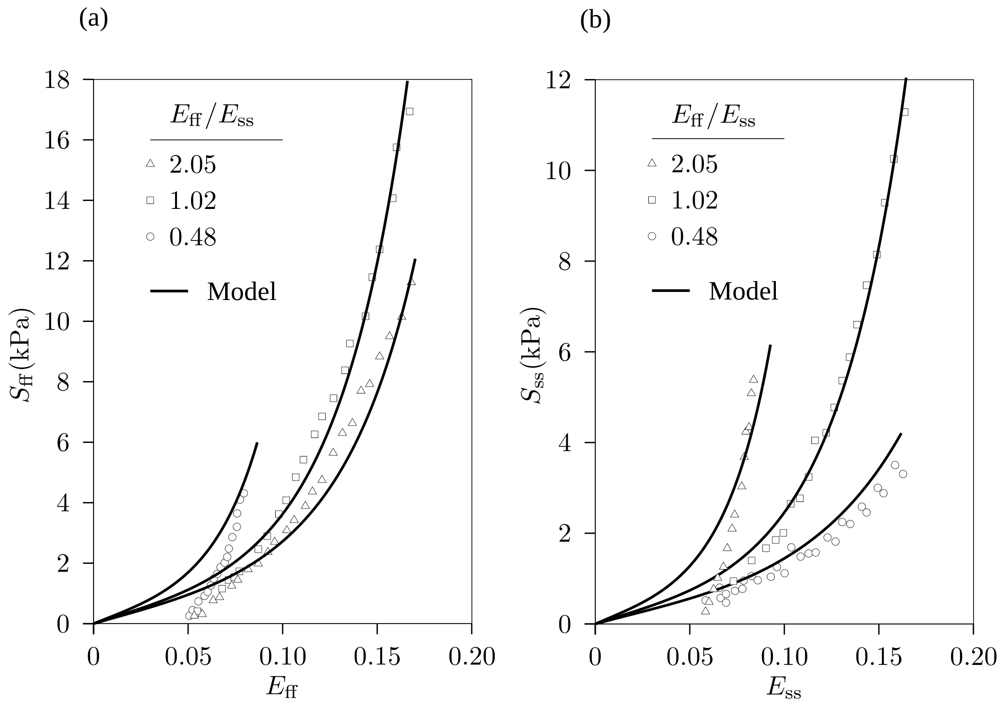

Figure 8. Fit of the model (5.39) to the experimental data of figure 3 (extracted from Yin *et al.*, 1987) for three different loading protocols for biaxial loading in the fs plane: (a) stress $S_{\rm ff}$ against strain $E_{\rm ff}$ in the fibre direction; (b) stress $S_{\rm ss}$ against strain $E_{\rm ss}$ in the sheet (cross-fibre) direction. The three sets of experimental data are indicated by triangles, squares and circles, while the continuous curves represent the fitted model. The biaxial data can be captured by a transversely isotropic model, and hence only four material constants are required to fit the data. The material parameters used are given in table 1.

6. Convexity and related issues

In Holzapfel *et al.* (2000) we discussed the important issue of convexity of the strain-energy function and its role in ensuring material stability and physically meaningful and unambiguous mechanical behaviour. It is also important for furnishing desirable mathematical features of the governing equations that have, in particular, implications for numerical computation (see also Holzapfel *et al.*, 2004; Ogden, 2003, 2009, for further discussion of convexity and related inequalities). For the discussion here the form of the strain-energy function (5.38) has particular advantages since it is the sum of separate functions of different invariants, with no cross terms between the invariants involved. This enables the convexity status of each term to be assessed separately. We shall therefore consider in succession the three functions $\mathcal{F}(I_1), \mathcal{G}(I_{4\,\rm f})$ and $\mathcal{H}(I_{8\,\rm fs})$ as representative and examine their convexity as a function of the right Cauchy-Green tensor $\mathbf{C}$.

(i) *The function* $\mathcal{F}(I_1)$

First we note that

$$\frac{\partial \mathcal{F}(I_1)}{\partial \mathbf{C}} = \mathcal{F}'(I_1)\mathbf{I}, \quad \frac{\partial^2 \mathcal{F}(I_1)}{\partial \mathbf{C} \partial \mathbf{C}} = \mathcal{F}''(I_1)\mathbf{I} \otimes \mathbf{I}. \tag{6.1}$$

Local convexity of $\mathcal{F}(I_1)$ as a function of $\mathbf{C}$ requires that

$$\frac{\partial^2 \mathcal{F}(I_1)}{\partial \mathbf{C} \partial \mathbf{C}}[\mathbf{A}, \mathbf{A}] \equiv \mathcal{F}''(I_1)(\mathrm{tr}\mathbf{A})^2 \geq 0 \tag{6.2}$$

for all second-order tensors $\mathbf{A}$, from which we deduce that $\mathcal{F}''(I_1) \geq 0$. Note that strict convexity is not possible since $\mathbf{A}$ can be chosen so that $\mathrm{tr}\mathbf{A} = 0$. For the exponential function considered in (5.38), i.e.

$$\mathcal{F}(I_1) = \frac{a}{2b}\{\exp[b(I_1 - 3)] - 1\}, \tag{6.3}$$

this yields $ab \geq 0$. For a nontrivial function, however, we must have $ab > 0$. It is also easy to see that for the stress response (in simple tension, for example) to be exponentially increasing in the corresponding stretch we must have $b > 0$. Thus, we have $a > 0$ and $b > 0$.

(ii) *The function* $\mathcal{G}(I_{4\,\mathrm{f}})$

For $\mathcal{G}(I_{4\,\mathrm{f}})$ it follows from the definition of $I_{4\,\mathrm{f}}$ in $(5.1)_1$ that

$$\frac{\partial \mathcal{G}}{\partial \mathbf{C}} = \mathcal{G}'(I_{4\,\mathrm{f}})\mathbf{f}_0 \otimes \mathbf{f}_0, \quad \frac{\partial^2 \mathcal{G}}{\partial \mathbf{C} \partial \mathbf{C}} = \mathcal{G}''(I_{4\,\mathrm{f}})\mathbf{f}_0 \otimes \mathbf{f}_0 \otimes \mathbf{f}_0 \otimes \mathbf{f}_0. \tag{6.4}$$

Local convexity of $\mathcal{G}(I_{4\,\mathrm{f}})$ requires that

$$\frac{\partial^2 \mathcal{G}}{\partial \mathbf{C} \partial \mathbf{C}}[\mathbf{A}, \mathbf{A}] \equiv \mathcal{G}''(I_{4\,\mathrm{f}}[(\mathbf{A}\mathbf{f}_0) \cdot \mathbf{f}_0]^2 \geq 0 \tag{6.5}$$

for all second-order tensors $\mathbf{A}$. It follows that $\mathcal{G}$ is convex in $\mathbf{C}$ provided $\mathcal{G}''(I_{4\,\mathrm{f}}) \geq 0$.

For the exponential form

$$\mathcal{G}(I_{4\,\mathrm{f}}) = \frac{a_\mathrm{f}}{2b_\mathrm{f}}\{\exp[b_\mathrm{f}(I_{4\,\mathrm{f}} - 1)^2] - 1\} \tag{6.6}$$

we obtain

$$\mathcal{G}'(I_{4\,\mathrm{f}}) = a_\mathrm{f}(I_{4\,\mathrm{f}} - 1)\exp[b_\mathrm{f}(I_{4\,\mathrm{f}} - 1)^2], \tag{6.7}$$

$$\mathcal{G}''(I_{4\,\mathrm{f}}) = a_\mathrm{f}\exp[b_\mathrm{f}(I_{4\,\mathrm{f}} - 1)^2]\{1 + 2b_\mathrm{f}(I_{4\,\mathrm{f}} - 1)^2\}. \tag{6.8}$$

For extension in the fibre direction we have $I_{4\,\mathrm{f}} > 1$, and from (6.7) we deduce that for the material response associated with this term to stiffen in the fibre direction we must have

$a_\mathrm{f} > 0$ and $b_\mathrm{f} > 0$. Moreover, these inequalities imply that $\mathcal{G}''(I_{4\,\mathrm{f}}) > 0$ and hence $\mathcal{G}$ is a convex function (both in tension and compression). It can be shown similarly that the separable Fung-type model (4.7) is convex if the material constants it contains are positive.

Since the pole-zero model (4.8) is separable it can be treated on the same basis. For example, if we consider just the first term in (4.8) we may write

$$\mathcal{G}(I_{4\,\mathrm{f}}) = \frac{k_\mathrm{ff} E_\mathrm{ff}^2}{|a_\mathrm{ff} - |E_\mathrm{ff}|\,|^{b_\mathrm{ff}}}, \tag{6.9}$$

where $I_{4\,\mathrm{f}} = 1 + 2E_\mathrm{ff}$, and, with $k_\mathrm{ff} > 0$, $a_\mathrm{ff} > 0$ and $b_\mathrm{ff} > 0$ it is straightforward to show that this is convex for all E_ff if $0 < b_\mathrm{ff} \leq 1$ or $b_\mathrm{ff} \geq 2$. However, it is convex for all E_ff such that $|E_\mathrm{ff}| < a_\mathrm{ff}$ (which is a necessary restriction) irrespective of the value of $b_\mathrm{ff} > 0$.

Although the calculations are somewhat different (because the contributions of the different components E_{ij} are not separable) it is also easily shown that the Costa model (4.5)–(4.6) and similar Fung-type models are convex if the coefficients b_{ij} are positive. By contrast, some models are not in general convex, as is the case with the model (4.2) because of the influence of the term cubic in $\sqrt{I_4} - 1$ and the coupled term in I_1 and I_4.

(iii) *The function* $\mathcal{H}(I_{8\,\mathrm{fs}})$

Similar results hold for $\mathcal{H}(I_{8\,\mathrm{fs}})$. Using the definition $(5.3)_1$ we calculate

$$\frac{\partial \mathcal{H}}{\partial \mathbf{C}} = \frac{1}{2}\mathcal{H}'(I_{8\,\mathrm{fs}})(\mathbf{f}_0 \otimes \mathbf{s}_0 + \mathbf{s}_0 \otimes \mathbf{f}_0) \tag{6.10}$$

and

$$\frac{\partial^2 \mathcal{H}}{\partial \mathbf{C}\partial \mathbf{C}} = \frac{1}{4}\mathcal{G}''(I_{8\,\mathrm{fs}})(\mathbf{f}_0 \otimes \mathbf{s}_0 + \mathbf{s}_0 \otimes \mathbf{f}_0) \otimes (\mathbf{f}_0 \otimes \mathbf{s}_0 + \mathbf{s}_0 \otimes \mathbf{f}_0). \tag{6.11}$$

For an arbitrary second-order tensor $\mathbf{A}$ we have

$$\frac{\partial^2 \mathcal{H}}{\partial \mathbf{C}\partial \mathbf{C}}[\mathbf{A}, \mathbf{A}] \equiv \mathcal{H}''(I_{8\,\mathrm{fs}})[(\mathbf{A}\mathbf{f}_0) \cdot \mathbf{s}_0]^2, \tag{6.12}$$

and for convexity this must be non-negative for all $\mathbf{A}$. Thus, $\mathcal{H}$ is convex in $\mathbf{C}$ provided $\mathcal{H}''(I_{8\,\mathrm{fs}}) \geq 0$.

For the exponential form

$$\mathcal{H}(I_{8\,\mathrm{fs}}) = \frac{a_\mathrm{fs}}{2b_\mathrm{fs}}\left[\exp(b_\mathrm{fs} I_{8\,\mathrm{fs}}^2) - 1\right] \tag{6.13}$$

we obtain

$$\mathcal{H}''(I_{8\,\mathrm{fs}}) = a_\mathrm{fs} \exp[b_\mathrm{fs}(I_{8\,\mathrm{fs}} - 1)^2](1 + 2b_\mathrm{fs} I_{8\,\mathrm{fs}}^2) \tag{6.14}$$

so convexity is guaranteed if $a_\mathrm{fs} > 0$ and $b_\mathrm{fs} > 0$.

In the above discussion based separately on the invariants $I_1, I_{4\,\mathrm{f}}$ and $I_{8\,\mathrm{fs}}$ we have examined only the convexity of individual terms that contribute (additively) to the strain-energy function. If each such term is convex then the overall strain-energy function is convex. Note, however, that it is not necessary that each such contribution be convex provided any non-convex contribution is counteracted by the convexity of the other terms. The analysis of convexity is relatively straightforward for a compressible material, but for an incompressible material more care is needed because then not all components of $\mathbf{E}$ are independent. For discussion of different aspects of convexity, see, for example, Holzapfel *et al.* (2000), Ogden (2003) and Ogden (2009).

(iv) *Strong ellipticity and other inequalities*

The notion of convexity is different from, but closely related to, aspects of material stability, for discussions of which in the context of the mechanics of soft biological tissues we refer to Holzapfel *et al.* (2004), Ogden (2003) and Ogden (2009), for example, and references therein. Whether of not the *strong ellipticity condition* holds is one issue that arises in consideration of material stability. If it holds then the emergence of certain types of non-smooth deformations, for example, is precluded. For three-dimensional deformations analysis of the strong ellipticity condition is difficult, especially for anisotropic materials such as those considered here. Necessary and sufficient conditions for strong ellipticity to hold for isotropic materials are available for three dimensions but are very complicated; in two dimensions they are much more transparent, but their counterparts, even for transversely isotropic materials, are not available. For plane strain deformations the strong ellipticity condition has been analyzed in some detail by Merodio & Ogden (2002) and Merodio & Ogden (2003), respectively for incompressible and compressible fibre-reinforced elastic materials. Here we focus our brief discussion on the anisotropic contributions to the strain-energy function.

If we consider the term $\mathcal{G}(I_{4\,\mathrm{f}})$, for example, on its own then (Merodio & Ogden, 2002) strong ellipticity requires that the inequalities

$$\mathcal{G}'(I_{4\,\mathrm{f}}) + 2I_{4\,\mathrm{f}}\mathcal{G}''(I_{4\,\mathrm{f}}) > 0, \quad \mathcal{G}'(I_{4\,\mathrm{f}}) > 0 \tag{6.15}$$

hold. From (5.22) and the formula $\mathbf{f}\cdot\mathbf{f} = I_{4\,\mathrm{f}}$, which comes from $(5.1)_1$, it can be seen that the component of Cauchy stress in the fibre direction is given by $2I_{4\,\mathrm{f}}\mathcal{G}'(I_{4\,\mathrm{f}})$. For this to be positive (negative) when $I_{4\,\mathrm{f}} > 1\,(< 1)$ we require $\mathcal{G}'(I_{4\,\mathrm{f}}) > 0\,(< 0)$, which means that strong ellipticity does not hold under fibre compression (this is the case for the exponential model; see equation (6.7)). In the context of arterial wall mechanics (see, for example, Holzapfel *et al.*, 2000) this problem is circumvented by recognizing that the fibres tend to buckle in compression and do not support compression to a significant degree, so that the term $\mathcal{G}(I_{4\,\mathrm{f}})$ can be considered to be inactive when $I_{4\,\mathrm{f}} < 1$. Even if this term is not dropped for compression in the fibre direction its tendency to lead to loss of ellipticity is moderated to some extent by the other terms in the strain-energy function. Turning now to the first inequality in (6.15) we note that this is equivalent to requiring that the nominal stress component in the fibre direction be a monotonic function of the stretch $\sqrt{I_{4\,\mathrm{f}}}$ in that direction, as shown by Merodio & Ogden (2002), which is consistent with the typical stiffening of the stress response of the fibres.

The situation with regard to $\mathcal{H}(I_{8\,\mathrm{fs}})$ is more delicate since, on its own, it can violate strong ellipticity in either tension or compression and generally has a destabilizing influence (Merodio & Ogden, 2006). Here we examine its behaviour for simple shear. With reference to (5.22) we note that $\mathcal{H}(I_{8\,\mathrm{fs}})$ contributes the term $\mathcal{H}'(I_{8\,\mathrm{fs}})(\mathbf{f}\otimes\mathbf{s}+\mathbf{s}\otimes\mathbf{f})$ to the Cauchy stress $\boldsymbol{\sigma}$. For the simple shear (sf) in the fs plane, we have $\mathbf{f}=\mathbf{f}_0$ and $\mathbf{s}=\gamma\mathbf{f}_0+\mathbf{s}_0$, where $I_{8\,\mathrm{fs}}=\gamma$ is the amount of shear; see §5(a)(i). The component of the shear stress on the plane normal to the initial direction $\mathbf{s}_0$ is then simply $\sigma_{12}=\mathcal{H}'(I_{8\,\mathrm{fs}})$, and we require

$$\mathcal{H}'(\gamma) \gtreqless 0 \quad \text{according as} \quad \gamma \gtreqless 0, \tag{6.16}$$

for the shear stress and strain to be in the same direction. Furthermore, if we require σ_{12} to be a monotonic increasing function of γ then we must have $\mathcal{H}''(I_{8\,\mathrm{fs}}) \geq 0$, which is consistent with the requirement of convexity in (iii) above.

7. Discussion

In order to understand the highly nonlinear mechanics of the complex structure of the passive myocardium under different loading regimes a rationally based continuum model is essential. In the literature to date models of the myocardium have been mainly of polynomial and/or exponential form, an important exception being the pole-zero model (4.8). Many of the models, including recently published ones, have been based on the assumption of transverse isotropy, and are not therefore able to capture the orthotropic response illustrated in the shear data of Dokos *et al.* (2002) on the myocardium. Moreover, not all of these are consistent with convexity requirements noted in §6; an example of such is (4.2), as mentioned in §6. As for the orthotropic models presented in §4(b) we have already noted the common feature that they are expressed in terms of the components of the Green–Lagrange strain tensor and that these particular components are also expressible in terms of the invariants. Thus, they all fit within the general framework we have outlined in §5. Note, however, that none of them has an explicit isotropic contribution.

While the Costa *et al.* (2001) model (4.5)–(4.6) has seven material parameters the model (4.7) has 12 and the pole-zero model in its most general form (4.8) has 18. However, the first of these three models has the disadvantage that the parameters are highly coupled and hence difficult to interpret in terms of the myocardium structure. As pointed out by Schmid *et al.* (2008) the parameter estimation process for the strain-energy function of Costa *et al.* (2001) was reliable, while for (4.7) and the special case of (4.8) with 12 parameters the process was unstable and required more sophisticated strategies, as outlined in their paper. It should be pointed out that, in general, least squares optimization procedures with large numbers of parameters can lead to non-uniqueness of parameter sets because of sensitivity to small changes in the data (see, for example, Fung, 1993, Section 8.6.1). Another common feature is that the orthotropic models reviewed here are somewhat *ad hoc* in nature and were constructed without the benefit of the general underlying theory such as that described in §5. Nevertheless, in spite of some shortcomings, including lack of convexity in some cases, these models have certainly been helpful in establishing some understanding of the biomechanics of the myocardium.

The specific constitutive model proposed in (5.38) has been shown to describes the general characteristics of the available biaxial data relatively well and to fit the available shear data very well. This is a model with only four invariants that is included within the general framework based on six independent invariants for an incompressible orthotropic material, which the myocardium is considered to be. A particular merit of the invariant theory is that it is geometry independent and requires knowledge only of the local preferred directions in the material. Moreover, it is relatively easy to implement within a finite element environment, as is the case with the invariant-based models for arteries (see, for example, Holzapfel, 2000). The three-dimensional orthotropic model is based on a structural approach in that it takes account of the morphological structure through the muscle fibre direction, the myocyte sheet orientation and the sheet normal direction and considers the resulting macroscopic nature of the myocardium. In this sense it is not considered to be a micro-mechanically based model. The particular form of the model adopted here uses a set of *eight* material parameters whose interpretations can be based partly on the underlying histology. This number can be reduced to *five* if the neo-Hookean model is used as the isotropic term for fitting the biaxial data or for illustrating basic features of the different simple shear modes. Construction of the model has been greatly facilitated by the clear structure of the stress–deformation equations that follow from the general form (5.22) and its specializations such as (5.23)–(5.28). Furthermore, the model introduced here is consistent with standard inequalities required from considerations of convexity, strong ellipticity and material stability.

Although some aspects of the passive mechanical response of the myocardium seem to be well known, a carefully literature survey shows that there are insufficient experimental data available, and there is therefore a pressing need for more data to inform further development based on the framework discussed in the present work. In terms of the need to simulate the response of the myocardium structure, the next step in our work is to develop a numerical (finite element) realization of the model. Beyond that, with the need for more data emphasized, the constitutive model for the passive behaviour of the myocardium proposed herein may serve as a robust basis for the development of more advanced coupled models that incorporate, for example, active response (muscle contraction), signal transduction and electrophysiology.

The authors wish to thank Thomas Eriksson for his helpful comments on this work and for performing the curve fitting. Financial support for this research was partly provided through an International Joint Project grant from the Royal Society of London. This support is gratefully acknowledged.

References

Bischoff, J. E., Arruda, E. M. & Grosh, K. 2002 A microstructurally based orthotropic hyperelastic constitutive law. *J. Appl. Mech.* **69**, 570–579.

Costa, K. D., Holmes, J. W. & McCulloch, A. D. 2001 Modeling cardiac mechanical properties in three dimensions. *Philos. T. Roy. Soc. A* **359**, 1233–1250.

Costa, K. D., Hunter, P. J., Wayne, J. S., Waldman, L. K., Guccione, J. M. & McCulloch, A. D. 1996 A three-dimensional finite element method for large elastic deformations of ventricular mycardium: II–Prolate spheroidal coordinates. *J. Biomech. Eng.* **118**, 464–472.

Costa, K. D., May-Newman, K., Farr, D., ODell, W. G., McCulloch, A. D. & Omens, J. H. 1997 Three-dimensional residual strain in midanterior canine left ventricle. *Am. J. Physiol. Heart Circ. Physiol.* **273**, H1968–H1976.

Demer, L. L. & Yin, F. C. P. 1983 Passive biaxial mechanical properties of isolated canine myocardium. *J. Physiol. London* **339**, 615–630.

Demiray, H. 1972 A note on the elasticity of soft biological tissues. *J. Biomech.* **5**, 309–311.

Demiray, H. 1976 Stresses in ventricular wall. *J. Appl. Mech.* **98**, 194–197.

Dokos, S., Smaill, B. H., Young, A. A. & LeGrice, I. J. 2002 Shear properties of passive ventricular myocardium. *Am. J. Physiol. Heart Circ. Physiol.* **283**, H2650–H2659.

Frank, J. S. & Langer, G. A. 1974 The myocardial interstitium: its structure and its role in ionic exchange. *J. Cell Biol.* **60**, 586–601.

Fung, Y. C. 1993 *Biomechanics. Mechanical properties of living tissues*, 2nd Edition. New York: Springer–Verlag.

Gilbert, S. H., Benson, A. P., Li, P. & Holden, A. V. 2007 Regional localisation of left ventricular sheet structure: integration with current models of cardiac fibre, sheet and band structure. *Eur. J. Cardiothorac. Surg.* **32**, 231–249.

Guccione, J. M., McCulloch, A. D. & Waldman, L. K. 1991 Passive material properties of intact ventricular myocardium determined from a cylindrical model. *J. Biomech. Eng.* **113**, 42–55.

Holzapfel, G. A. 2000 *Nonlinear solid mechanics. A continuum approach for engineering*. Chichester: John Wiley & Sons.

Holzapfel, G. A., Gasser, T. C. & Ogden, R. W. 2000 A new constitutive framework for arterial wall mechanics and a comparative study of material models. *J. Elasticity* **61**, 1–48.

Holzapfel, G. A., Gasser, T. C. & Ogden, R. W. 2004 Comparison of a multi-layer structural model for arterial walls with a Fung-type model, and issues of material stability. *J. Biomech. Eng.* **126**, 264–275.

Holzapfel, G. A. & Ogden, R. W. 2003 *Biomechanics of soft tissue in cardiovascular systems*. CISM Courses and Lectures, no. **441**. Wien, New York: Springer–Verlag.

Holzapfel, G. A. & Ogden, R. W. 2009 *Biomechanical modelling at the molecular, cellular and tissue levels*. CISM Courses and Lectures, no. **508**. Wien, New York: Springer–Verlag.

Holzapfel, G. A. & Ogden, R. W. In press. On planar biaxial tests for anisotropic nonlinearly elastic solids. A continuum mechanical framework. *Math. Mech. Solids*. (doi:10.1177/1081286507084411).

Horowitz, A., Lanir, Y., Yin, F. C. P., Perl, M., Sheinman, I. & Strumpf, R. K. 1988 Structural three-dimensional constitutive law for the passive myocardium. *J. Biomech. Eng.* **110**, 200–207.

Humphrey, J. D., Strumpf, R. K. & Yin, F. C. P. 1990 Determination of constitutive relation for passive myocardium: I. A new functional form. *J. Biomech. Eng.* **112**, 333–339.

Humphrey, J. D. & Yin, F. C. P. 1987 On constitutive relations and finite deformations of passive cardiac tissue – Part I: A pseudo-strain energy function. *J. Biomech. Eng.* **109**, 298–304.

Hunter, P. J., Nash, M. P. & Sands, G. B. 1997 Computational electromechanics of the heart. In *Computational biology of the heart* (eds A. V. Panfilov & A. V. Holden), pp. 345–407. Chichester: John Wiley & Sons.

Huyghe, J. M., Arts, T., van Campen, D. H. & Reneman, R. S. 1992 Porous medium finite element model of the beating left ventricle. *Am. J. Physiol. Heart Circ. Physiol.* **262**, H1256–H1267.

Huyghe, J. M., van Campen, D. H., Arts, T. & Heethaar, R. M. 1991 The constitutive behaviour of passive heart muscle tissue. A quasi-linear viscoelastic formulation. *J. Biomech.* **24**, 841–849.

Katz, L. N. 1977 *Physiology of the heart*. New York: Raven Press.

Kerckhoffs, R. C. P., Bovendeerd, P. H. M., Kotte, J. C. S., Prinzen, F. W., Smits, K. & Arts, T. 2003 Homogeneity of cardiac contraction despite physiological asynchrony of depolarization: A model study. *Ann. Biomed. Eng.* **31**, 536–547.

LeGrice, I. J., Hunter, P. J. & Smaill, B. H. 1997 Laminar structure of the heart: a mathematical model. *Am. J. Physiol. Heart Circ. Physiol.* **272**, H2466–H2476.

LeGrice, I. J., Smaill, B. H., Chai, L. Z., Edgar, S. G., Gavin, J. B. & Hunter, P. J. 1995 Laminar structure of the heart: Ventricular myocyte arrangement and connective tissue architecture in the dog. *Am. J. Physiol. Heart Circ. Physiol.* **269**, H571–H582.

MacKenna, D. A., Omens, J. H. & Covell, J. W. 1996 Left ventricular perimysial collagen fibers uncoil rather than stretch during diastolic filling. *Basic Res. Cardiol.* **91**, 111–122.

Merodio, J. & Ogden, R. W. 2002 Material instabilities in fiber-reinforced nonlinearly elastic solids under plane deformation. *Arch. Mech.* **54**, 525–552.

Merodio, J. & Ogden, R. W. 2003 Instabilities and loss of ellipticity in fiber-reinforced compressible nonlinearly elastic solids under plane deformation. *Int. J. Solids Structures* **40**, 4707–4727.

Merodio, J. & Ogden, R. W. 2006 The influence of the invariant I_8 on the stress.deformation and ellipticity characteristics of doubly fiber-reinforced non-linearly elastic solids. *Int. J. Non-Linear Mech.* **41**, 556–563.

Nash, M. P. 1998 *Mechanics and material properties of the heart using an anatomically accurate mathematical model*. Ph.D. thesis, The University of Auckland, New Zealand.

Novak, V. P., Yin, F. C. P. & Humphrey, J. D. 1994 Regional mechanical properties of passive myocardium. *J. Biomech. Eng.* **27**, 403–412.

Ogden, R. W. 1997 *Non-linear elastic deformations*. New York: Dover Publications.

Ogden, R. W. 2003 Nonlinear elasticity, anisotropy and residual stresses in soft tissue. In *Biomechanics of soft tissue in cardiovasular systems* (eds G.A. Holzapfel & R.W. Ogden), pp. 65–108. CISM Courses and Lectures, no. **441**. Wien, New York: Springer–Verlag.

Ogden, R. W. 2009 Anisotropy and nonlinear elasticity in arterial wall mechanics. In *Biomechanical modelling at the molecular, cellular and tissue levels* (eds G.A. Holzapfel & R.W. Ogden), pp. 179–258. CISM Courses and Lectures, no. **508**. Wien, New York: Springer–Verlag.

Omens, J. H. & Fung, Y. C. 1990 Residual strain in rat left ventricle. *Circ. Res.* **66**, 37–45.

Rachev, A. 1997 Theoretical study of the effect of stress-dependent remodeling on arterial geometry under hypertensive conditions. *J. Biomech.* **30**, 819–827.

Rodriguez, E. K., Hoger, A. & McCulloch, A. D. 1994 Stress-dependent finite growth in soft elastic tissues. *J. Biomech.* **27**, 455–467.

Sands, G. B., Gerneke, D. A., Hooks, D. A., Green, C. R., Smaill, B. H. & LeGrice, I. J. 2005 Automated imaging of extended tissue volumes using confocal microscopy. *Microsc. Res. Tech.* **67**, 227–239.

Schmid, H., Nash, M. P., Young, A. A. & Hunter, P. J. 2006 Myocardial material parameter estimation-a comparative study for simple shear. *J. Biomech. Eng.* **128**, 742–750.

Schmid, H., O'Callaghan, P., Nash, M. P., Lin, W., LeGrice, I. J., Smaill, B. H., Young, A. A. & Hunter, P. J. 2008 Myocardial material parameter estimation: a non-homogeneous finite element study from simple shear tests. *Biomech. Model. Mechanobiol.* **7**, 161–173.

Smaill, B. H. & Hunter, P. J. 1991 Structure and function of the diastolic heart: material properties of passive myocardium. In *Theory of heart: biomechanics, biophysics, and nonlinear dynamics of cardiac function* (eds L. Glass, P. J. Hunter & A. D. McCulloch), pp. 1–29. New York: Springer–Verlag.

Spencer, A. J. M. 1984 Constitutive theory for strongly anisotropic solids. In *Continuum theory of the mechanics of fibre-reinforced composites* (ed. A. J. M. Spencer), pp. 1–32. CISM Courses and Lectures no. **282**. Wien: Springer–Verlag.

Vossoughi, J., Vaishnav, R. N. & Patel, D. J. 1980 Compressibility of the myocadial tissue. In *Advances in Bioengineering* (ed. Van C. Mow), pp. 45–48. New York: Bioengineering Division, American Society of Mechanical Engineers.

Yin, F. C. P. 1981 Ventricular wall stress. *Circ. Res.* **49**, 829–842.

Yin, F. C. P., Strumpf, R. K., Chew, P. H. & Zeger, S. L. 1987 Quantification of the mechanical properties of noncontracting canine myocardium under simultaneous biaxial loading. *J. Biomech.* **20**, 577–589.

Young, A. A., Legrice, I. J., Young, M. A. & Smaill, B. H. 1998 Extended confocal microscopy of myocardial laminae and collagen network. *J Microsc.* **192**, 139–150.